Miner Deposita (2007) 42:913–935
DOI 10.1007/s00126-007-0142-6

ARTICLE

Geochemical constraints on the origin of the Kicking Horse and Monarch Mississippi Valley-type lead-zinc ore deposits, southeast British Columbia, Canada

Veerle Vandeginste · Rudy Swennen · Sarah A. Gleeson · Rob M. Ellam · Kirk Osadetz · François Roure

Received: 19 July 2006 / Accepted: 12 May 2007 / Published online: 1 June 2007

Abstract Two Mississippi Valley-type (MVT) ore deposits, Kicking Horse and Monarch, have been studied with the aim of comparing the ores at the two localities and to characterize the origin of the mineralizing fluids and the ore formation process(es). Both deposits are hosted by the Middle Cambrian Cathedral Formation carbonate host rocks, Kicking Horse on the north and Monarch on the south flank of the Kicking Horse valley near Field (SE British Columbia). The ore bodies are situated at the transition of (western) basinal to (eastern) shallow-water strata of the paleo-Pacific passive margin succession in the Cordilleran Foreland Province of the Western Canada Sedimentary Basin. Both deposits are related spatially to normal faults. In both localities, the ore minerals are dominated by pyrite, sphalerite, and galena. Dolomite, minor quartz, and calcite are also present in close association with the ores. The salinity (21–30 wt% NaCl eq.) and homogenization temperatures (63–182°C) measured in fluid inclusions in carbonate, quartz, and sphalerite lie within the typical range of MVT fluid conditions. The good stoichiometry (50–53 mol% $CaCO_3$), low $\delta^{18}O$ values (−21 to −14‰ Vienna Peedee belemnite) and relatively high homogenization temperatures (>95°C) of the dolomite suggest the dolomites were formed under burial diagenesis. The ore-forming fluids probably interacted with siliciclastic units, based on elevated Li contents and $^{87}Sr/^{86}Sr$ ratios, which are highest in the dolomite type after the main ore stage. We propose that the ores formed from the mixing of a downward-infiltrating, sulfur-bearing halite-dissolution fluid with an upward-migrating, metal-rich evaporated seawater fluid, which had already undergone minor mixing with a dilute fluid.

Keywords Mississippi Valley-type · Lead–zinc · Fluid inclusions · Kicking Horse · Monarch · Canada

Editorial handling: B. Lehmann

V. Vandeginste (✉) · R. Swennen
Afdeling Geologie,
Katholieke Universiteit Leuven,
Celestijnenlaan 200E,
3001 Heverlee, Belgium
e-mail: Veerle.Vandeginste@gmail.com

S. A. Gleeson
Department of Earth and Atmospheric Sciences,
University of Alberta,
Edmonton, Alberta, Canada, T6G 2E3

R. M. Ellam
Scottish Universities Environmental Research Centre,
Rankine Avenue,
East Kilbride G750QF, UK

K. Osadetz
Geological Survey of Canada,
3303-33rd Street N.W.,
Calgary, Alberta, Canada, T2L 2A7

F. Roure
Institut Français du Pétrole,
1 and 4, Avenue de Bois-Préau,
92852 Rueil-Malmaison Cedex, France

Introduction

Mississippi Valley-type (MVT) deposits are epigenetic, carbonate-hosted Pb–Zn deposits that are thought to be formed in and adjacent to sedimentary basins from basinal brines (e.g., Hanor 1996; Leach et al. 2001; Viets et al. 1996). These deposits are formed from high salinity fluids (~16–26 wt% $CaCl_2$ eq.) at temperatures between ~75 and 150°C (e.g., Basuki and Spooner 2004; Leach et al. 2005;

Wilkinson 2001). In Western Canada, several important MVT ore deposits occur including Pine Point, Robb Lake, and Gayna River (e.g., Leach et al. 2001). In addition, some smaller MVT Pb–Zn occurrences are found in the Western Canadian foreland fold-and-thrust belt including the Kicking Horse and Monarch deposits and also Eldon, Baker Creek, and Hawk Creek (e.g., Evans et al. 1968; Holter 1977). In the Western Canada Sedimentary Basin, the base metal mineralization is closely associated with the formation of coarse dolomite cements (e.g., Nesbitt and Muehlenbachs 1994).

The genetic link between the regional formation of sulfide ores and dolomite cements has been the subject of several fluid flow models. Proposed models include topographically driven fluid flow (Garven 1985; Yao and Demicco 1995, 1997), tectonically driven fluid flow (Machel and Cavell 1999), and thermally convective fluid flow (Nelson et al. 2002). However, the formation of the individual deposits and also the age of migration of the mineralizing fluids in the Western Canada Sedimentary Basin is still much debated.

This study focuses on two of the carbonate-hosted Pb–Zn deposits in Western Canada, the Kicking Horse and Monarch ore deposits, which have been previously described as MVT lead–zinc deposits (e.g., Evans et al. 1968; Leach et al. 2001). The Kicking Horse and Monarch ore deposits are located 5 km northeast of Field in Yoho National Park, British Columbia. The NNW–SSE-aligned Pb–Zn deposits occur approximately 1 km apart and are located at the carbonate–shale facies change of the Paleozoic passive margin succession. The deposits are also associated with normal faults (Fig. 1). Both the facies transition, known as the Kicking Horse Rim (Aitken 1971), and the normal faults, in particular the Stephen–Cathedral and the Fossil Gully faults, have a NNW–SSE orientation. Between 1912 and 1952, about 860,000 tons of Pb (7%)–Zn (10%) ores (with 34 g Ag/ton) were produced (Ney 1954). The Kicking Horse and

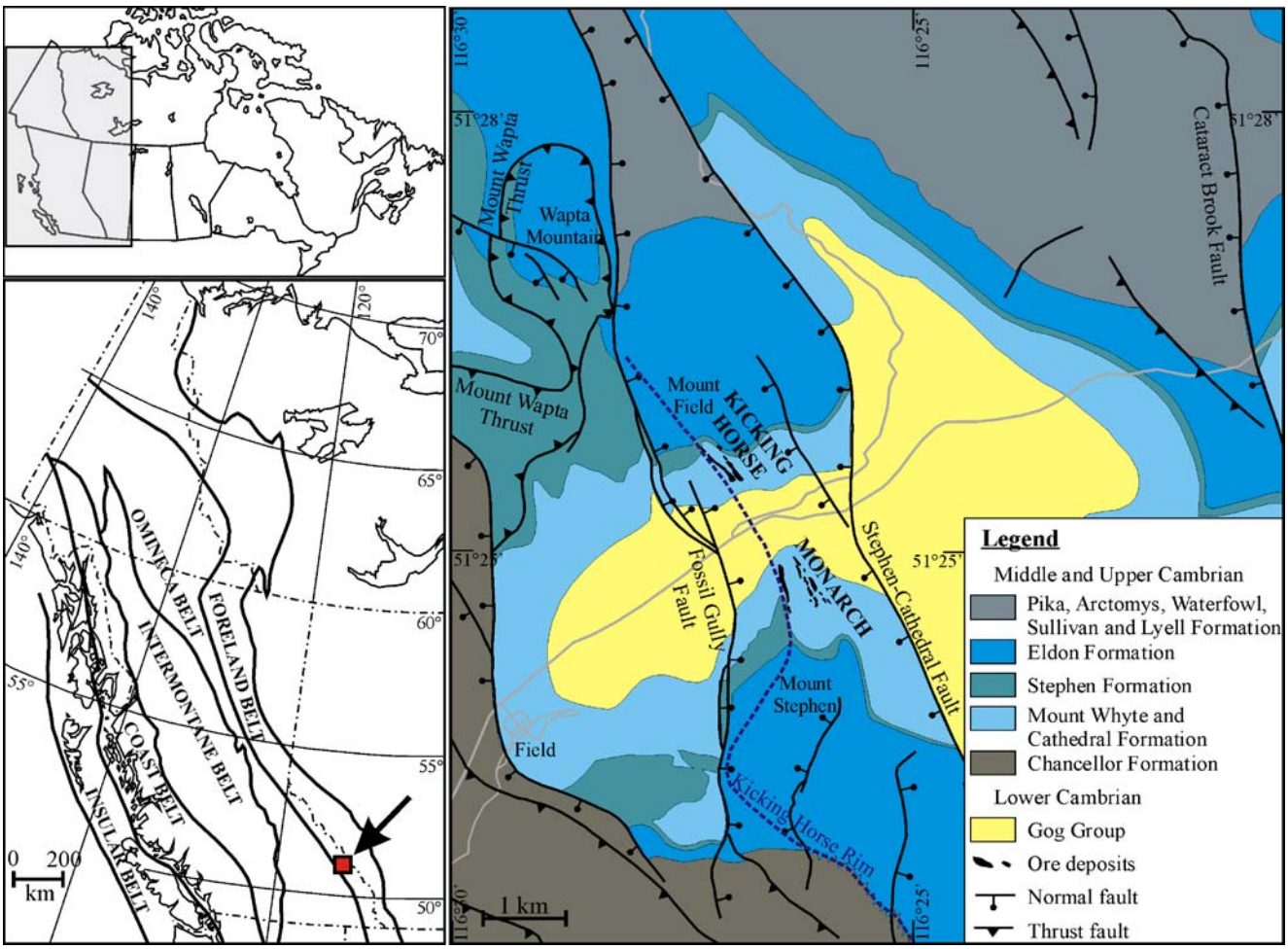

Fig. 1 A map of Canada with a *rectangle* indicating a view of Western Canada with the morphological belts of the Canadian Cordillera in the *bottom left corner*. The *red square*, indicated with an *arrow*, shows the location of the geological map (on the *right*) of the study area (after Price et al. 1980). The *black elongated bodies* on Mount Field and Mount Stephen indicate the location of the ore zones (as represented in Symons et al. 1998)

Monarch mineralization was the subject of several previous studies (e.g., Allan 1914; Brown 1948; Goranson 1937; Ney 1954), which focused on macroscopic observations including the local geology, mineralogy, structures, and mine workings. More recent regional studies on MVT ore and/or dolomite in the Western Canada Sedimentary Basin incorporated limited geochemical or fluid inclusion analyses on samples from Kicking Horse and/or Monarch, e.g., mineralogy, geochemistry, and sulfur isotopes of Western Canadian Pb–Zn deposits by Evans et al. (1968), fluid inclusion data, stable carbon, oxygen and hydrogen isotopes, and $^{87}Sr/^{86}Sr$ analyses by Nesbitt and Muehlenbachs (1994), and fluid inclusion crush–leach analyses of dolomite of the Kicking Horse and Monarch mineralization and other dolomite and magnesite samples from the southern Canadian Rockies by Nesbitt and Prochaska (1998). A paleomagnetic study on ore and dolomite from the Kicking Horse and Monarch localities was carried out by Symons et al. (1998).

The Kicking Horse and Monarch ore deposits were interpreted previously to have formed simultaneously based on the proximity and orientation of the ore bodies. Goranson (1937) and Brown (1948) proposed that ore-bearing solutions probably had migrated along or near the Stephen–Cathedral fault, and Ney (1954) hypothesized a hydrothermal origin for the Cathedral dolomite, which preceded the ore mineralization by fluids that either advanced longitudinally from a source located in the Kicking Horse valley or migrated upward along a structure, such as the Stephen–Cathedral fault.

Noteworthy is the occurrence of (zebra) burial dolomite host rocks within 5 km of the Kicking Horse and Monarch deposits. The zebra dolostones have been interpreted to have formed by tectonically driven focused fluid flow (Vandeginste et al. 2005).

We focus on both the Kicking Horse and Monarch deposits to investigate the geochemistry of the ore-forming solutions and to attempt to constrain the ore-forming process. We report on mineralogical characteristics, carbonate geochemistry, carbonate carbon, oxygen, and strontium isotopic signatures, fluid inclusion microthermometry, and the crush–leach geochemistry of sulfides and carbonates from these two ore deposits. This is the first detailed geochemical study of the various mineral types of the paragenetic sequence at both the Kicking Horse and Monarch deposits. Our results are compared with data from dolomite from the Western Canada Sedimentary Basin and with ore-related minerals from Pine Point and other MVT deposits in the Canadian Cordilleran foreland belt.

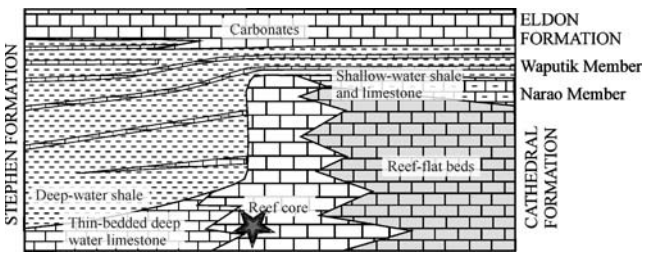

Fig. 2 Sketch of the Middle Cambrian lithologies and stratigraphic units at the Kicking Horse Rim (after Aitken 1997). The *star* indicates the approximate position of the Kicking Horse and Monarch deposits

Geological setting

The Kicking Horse and Monarch ore deposits are located in the Rocky Mountains foreland fold-and-thrust belt, which is the most easterly deformed belt of the Canadian Cordillera (Fig. 1). The latter consists of an accretionary prism formed as the result of convergent tectonics at the western border of the North American protocontinent with several oceanic plates and allochthonous terranes. Several orogenic events have affected this region: the Middle Devonian Antler Orogeny (Root 2001) and Cordilleran orogenic phases, the Late Jurassic–Early Cretaceous Columbian phase, and the Late Cretaceous–Paleocene Laramide phase. The present day fold-and-thrust belt is characterized by an abundance of SW-dipping, NW–SE-oriented thrust faults, which bifurcate cratonward from a basal detachment fault system, which commonly lies throughout most of the Foreland Belt, approximately at the contact between the sedimentary rocks and the crystalline basement. While the western zone of the fold-and-thrust belt in the study area consists mainly of shales and argillaceous limestones of the Cambrian and Ordovician age, the strata east of the Kicking Horse Rim are dominated by carbonate of the Paleozoic age, Jurassic siliciclastic formations, and farther to the east, Cretaceous clastic sequences are exposed. The Kicking Horse Rim is a paleogeographic feature defined by Aitken (1978, 1997) as a narrow carbonate shoal complex, active during the Middle and Upper Cambrian and probably into the Ordovician, consisting of peritidal strata, lying west of subtidal platform deposits and east of strata of basinal and slope origin (Fig. 2). The Kicking Horse and the Monarch ore deposits are located where the Middle Cambrian Stephen Formation thins abruptly to the east (Fig. 1 and 2). The cigar-shaped ore bodies lie flat and are elongated in the top of a broad anticline (Cook 1975). They occur in the footwall block parallel to two normal faults. Furthermore, they appear just above the contact with black dolomite and overlying light gray dolomite breccia of the Middle Cambrian Cathedral Formation (Brown 1948; Fig. 3). According to Brown (1948), this breccia, which is confined to the area within the fault block, has a tectonic origin. The brecciated dolomite consists of either light gray dolomite fragments in dark gray dolomite or a stockwork of coarse white dolomite veins in gray dolomite (Ney 1954). The first breccia type occurs as a halo varying in thickness from one third, to several times the width of the ore body, and is found above and lateral to the ore zone,

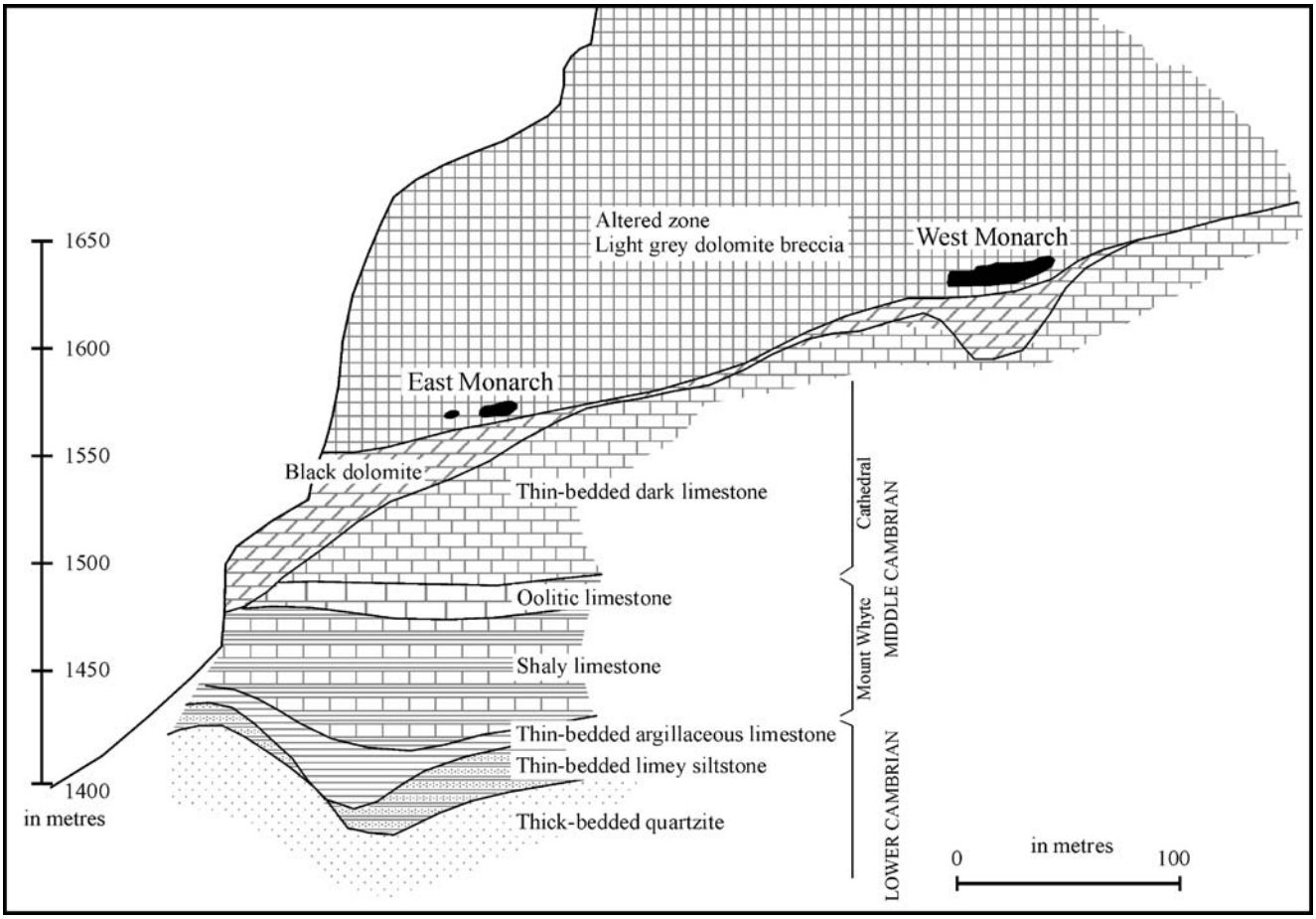

Fig. 3 Cross-section through Mount Stephen with Monarch Mines (after Ney 1954). The Stephen–Cathedral fault passes in the valley at the *left side* of the picture

whereas the stockwork dolomite breccia is widespread and can be found throughout the altered Cathedral Formation (Ney 1954). Ney (1954) suggested that the ideal ore-bearing material has a major development of gray breccia, with 15–30% veinlets of the stockwork breccia type. An origin for the breccia types was not proposed by Ney (1954). Harrison and McIlreath (1977) suggested that the galena, sphalerite, and pyrite in the deposits either replace the light gray dolomite breccia or occur as sulfide veinlets. The top of the brecciated zone grades into light gray structureless dolomite, which, in turn, grades into banded gray to black crystalline dolomite (Goranson 1937).

Materials and methods

The mines are long abandoned, and the entrances to the mine workings are currently closed and inaccessible. No samples of the ores were found in situ at accessible outcrops. Therefore, sulfide and carbonate samples were collected from loose blocks in front of the old mine adits on Mount Field and Mount Stephen (Fig. 1) and may not be representative of the ore in place in the mines. Nevertheless, the samples do include examples similar to the ores described by Ney (1954). Clear structural relationships between the ore samples could not be defined; therefore, we relied on published ore descriptions for micro- and mesoscale structures and relationships. In addition, an aerial photographic analysis was carried out to identify any macroscale structures in the vicinity of the mines.

Finely polished and etched rock slabs and thin sections were stained with Alizarin Red S and potassium ferricyanide to distinguish calcite and dolomite and their ferroan equivalents. Sulfide minerals were etched with a solution of 0.1 M $KMnO_4$ and 0.1 M H_2SO_4 (Ramdohr 1969) to reveal potential zonation patterns.

For cathodoluminescence (CL) microscopy, unstained thin sections were used. A cold cathode luminoscope (Technosyn Model 8200 Mark II) was used for the observation of most thin sections with a beam voltage of 17 kV and a current of 600 μA. A hot cathode luminoscope (HC3-LM type) was used for the observation of sphalerite and quartz under a maximum voltage of 14 kV and beam current of 0.2 mA.

X-ray diffraction (XRD) analyses of carbonate powders, using an internal halite standard, were performed with a Phillips PW1130 type XRD machine at a scan speed of 0.5°2θ/min with a sampling interval of 0.01°2θ/step and Co-Kα radiation at 30 kV and 20 mA. Stoichiometry of dolomite was determined following the equation of Lumsden (1979), and cation ordering was determined by peak width, i.e., full width at half maximum, and expressed in °2θ.

Major (Mg, Ca) and trace-element (Na, Sr, Fe, Mn, K, Zn, Cu, Pb) compositions of carbonate were measured by atomic absorption spectrometry (AAS). A microscopic study preceded the selection of the carbonate samples to select suitable sample material. Moreover, representative samples were studied with the scanning electron microscopy and energy-dispersive X-ray analysis (SEM–EDX) to exclude a significant influence of potential solid inclusions on the chemical analyses of carbonate. The clean, hand-picked carbonate samples were then crushed in a mortar, and their powders were dried in an oven at 100°C overnight. Subsequently, 1 g of each carbonate powder was dissolved in 40 ml 1 M HCl, and the solution was evaporated at 60°C. Then, another 20 ml 1 M HCl was added, and the solution was filtered before measuring major and trace element contents as well as the HCl-insoluble residue (IR) content. Analytical precision determined on replicate analyses was better than 10% (2σ).

For carbon and oxygen isotope analyses of carbonate, a few milligrams of the sample was drilled out and analyzed at the University of Erlangen (Germany). Carbonate powders were reacted with 100% phosphoric acid (density >1.9 g/cm^3, Wachter and Hayes 1985) at 75°C in a carbonate preparation line (Carbo–Kiel single-sample acid bath) connected to a Finnigan Mat 252 mass spectrometer. All values are reported in per mil relative to Vienna Peedee belemnite (VPDB) by assigning a δ^{13}C value of +1.95‰ and a δ^{18}O value of −2.20‰ to NBS19. The oxygen isotopic composition of dolomite was corrected using the fractionation factors given by Rosenbaum and Sheppard (1986). Reproducibility was checked by replicate analysis of laboratory standards and was better than ±0.03‰ for δ^{13}C (1σ) and ±0.04‰ for δ^{18}O (1σ).

Sr isotope analyses were carried out at the Scottish Universities Environmental Research Centre (Scotland). Carbonate samples were leached in 1 N NH_4Ac before acid digestion in 2.5 M HCl. Sr was separated in 2.5 M HCl using Bio-Rad AG50W X8 200–400 mesh cation exchange resin. Total procedure blank for Sr samples prepared using this method is less than 200 pg. Sr was analyzed with a VG Sector 54–30 multiple collector mass spectrometer, and samples were loaded onto single Ta filaments with 1 N phosphoric acid. A ^{88}Sr intensity of 1 V (1×10^{-11} A)±10% was maintained, and the ^{87}Sr/^{86}Sr ratio was corrected for mass fractionation using $^{86}Sr/^{88}Sr = 0.1194$ and an exponential law. The mass spectrometer was operated in the peak-jumping mode with data collected as 15 blocks of ten ratios. For this instrument, NIST SRM987 gave 0.710258±11 (1σ, n=16) during the course of this study.

Fluid inclusions in doubly polished wafers were studied microthermometrically on a Linkam THMSG 600 heating-cooling stage. Calibration of the stage between −56.6 and 374.1°C was performed by measuring phase changes in synthetic fluid inclusions of known composition. Reproducibility of the final melting temperature of ice (Tm_{ice}) was within ±0.2°C and of the homogenization temperature (Th) within ±2°C. Homogenization temperatures were determined before melting temperatures in carbonate and in sphalerite, whereas this was reversed for the measurements in quartz. The Th values presented in the text have not been corrected for pressure. Such a pressure correction is minor; that is, for a minimum depth of 2 km for dolomite precipitation, the real trapping temperature correction is in the order of 10 to 20°C, as calculated for a hydrostatic to lithostatic fluid pressure using isochores of the samples studied.

Samples that had been well constrained in the microthermometric study and could be shown to be dominated by one population of fluid inclusions were chosen for the crush–leach analysis. In this study, the only sample that contained clear secondary fluid inclusions was the Kicking Horse reddish dolomite (see below). The occurrence of these secondary inclusions, however, was rare, and they had relatively low salinities. Therefore, it is likely that the influence of these secondary fluid inclusions on the bulk halogen analysis is minimal. Representative samples were, before crushing, studied with the SEM–EDX to confirm the purity of the samples and to exclude the presence of potential solid inclusions.

For crush–leach analyses (see Gleeson 2003), cleaned carbonate, quartz, and sulfide samples were crushed and sieved to obtain a 1–2-mm grain size fraction. The crushed samples were washed in ultraclean water, heated overnight on a hot plate, and then dried in an oven. One gram of sample was ground to a fine powder using an agate mortar and pestle. Half of the powder was transferred to an unreactive vial, and 5 ml of clean water was added. These samples were shaken and filtered through 0.2-μm filters to yield particulate-free leachate. Anions (Cl, Br, F, and sulfate) were then analyzed using a Dionex DX600 ion chromatograph, and Li, Na, and K were analyzed using AAS. Replicate analyses of standard solutions on the DX600 were within 4%. Accuracy, as measured by a commercial quality control solution analyzed in each run, was within 1%. Detection limits are 0.005 ppm for Cl and Br and 0.001 ppm for F and sulfate. A second leachate was prepared for a single quartz sample by leaching the sample powder with an acidified La-doped solution. This is used to prevent the divalent and trivalent cations adhering to the surface of the powder that would give

erroneous results (Bottrell and Yardley 1988). The La-doped leachates were analyzed using inductively coupled plasma mass spectrometry for Na, Ca, Fe, K, Mn, Pb, Zn, Sr, Ba, Al, B, Li, Co, As, Cd, Si, S, and Mg. Only the Ca, Na, K, and Mg data will be discussed for this quartz sample.

The leaching is carried out with pure water for the carbonate and sulfide minerals, but it is a possibility that minute solid inclusions of soluble or partially soluble minerals may affect the analytical results. However, the solubility of, for example, Al silicates in pure water is extremely low (no more than 5×10^{-7} mol muscovite can dissolve in water at room temperature), and as mentioned above, samples were checked for inclusions in the petrographic study. If submicroscopic inclusions were present in the sample, it is likely that the contribution of elements from these would be very small and much less than the contribution of the fluid inclusions to the leachates.

Petrography, mineralogy, and paragenesis

The petrographically deduced paragenesis is presented in Fig. 4. In addition to ore emplacement, the host rock was altered by major dolomite formation (cementation and replacement). Small occurrences of quartz, sericite, and calcite were detected in some samples (especially from the Kicking Horse locality). Multiple occurrences of pyrite, sphalerite, and galena were identified based on color, textural characteristics, and their mutual relationships. They are reported accordingly.

Host rock dolostone

Two types of dolomite constitute the host rocks for the mineralization, a fabric-preserving, fine-crystalline, dark dolomite, which is partially to completely replaced by a fabric-destructive gray dolomite comprised of relatively small (40–120 μm) nonplanar crystals. In samples from the ore zone, both dolomite types can occur as brecciated fragments that are surrounded by sphalerite and pyrite (Fig. 5a).

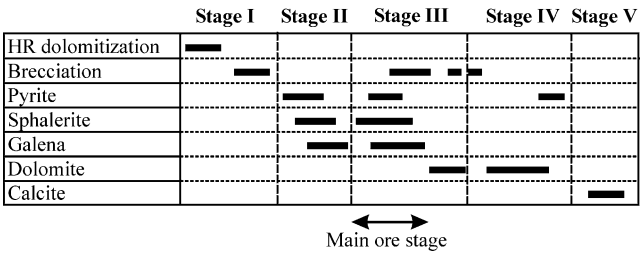

Fig. 4 Simplified paragenetic sequence for samples from the Kicking Horse and Monarch localities

Disseminated sulfide

The fine crystalline sulfide disseminated in the host rocks includes, in paragenetic order, small (40–120 μm), generally well-formed cubic pyrite crystals, brownish red and green sphalerite, and galena (Fig. 5b–d).

Nondisseminated sulfide and ore-associated carbonate

Nondisseminated forms of pyrite include cubic crystals, colloform bands, and massive crystals. Sphalerite can occur in finely crystalline bands of different color and texture (Fig. 5e), including a distinctive band of dark brownish green sphalerite with a granular-like structure, present in both the Kicking Horse and Monarch ores. This sphalerite appears to precede a dissolution collapse brecciation, and its fragments are enclosed by gray dolomite (Fig. 5f). Sphalerite sometimes surrounds brecciated host rock dolomite fragments. Sphalerite also occurs in colloform bands, alternating with pyrite and galena (Fig. 5g). Galena is present as small grains in sphalerite that cements brecciated dolomite fragments, in colloform bands, as massive units and locally fills vugs and available porosity (Fig. 5h). Generally, more sphalerite was found in samples from the Kicking Horse Mine, whereas more galena was found in samples from the Monarch Mine.

Etching of the samples did not reveal any zonation within the sulfide minerals. All sphalerites were nonluminescent under cold as well as hot CL.

Gray and white dolomites are found associated with sulfides. Both dolomites are characterized by 51–53 mol% $CaCO_3$ (based on XRD analysis, uncorrected for Fe content, Fig. 6). The dolomite consists of ferroan (as revealed by staining), coarse (up to several millimeters) nonplanar (infrequently elongated), or saddle dolomite crystals marked by undulose extinction under cross-polarized light. They often cement brecciated host rock dolomite fragments, but white dolomite can also be found in (stockwork) veins, especially at the Monarch locality. In addition, a transparent coarse-crystalline calcite (up to several millimeters), characterized by cleavage planes, occurs in small amounts adjacent to the dolomite.

Small amounts of quartz were observed with the gray dolomite at the Kicking Horse locality.

Late-coarse-crystalline pyrite and dolomite

Coarsely crystalline pyrite occurs late in the paragenesis in some samples. Also postdating the ore paragenetic stage are medium crystalline gray, white, reddish, and very coarse-crystalline white dolomite, all characterized by 50–51 mol% $CaCO_3$ (based on XRD analysis, uncorrected for Fe content, Fig. 6). The dolomite types were differentiated based on

color, texture, and CL characteristics (Table 1). These carbonates are also found as breccia cements and different stages of brecciation are associated with the different dolomite types. The breccias are dominantly monomict with rounded to angular light or dark gray host rock fragments. Some brecciated samples show evidence of evaporite pseudomorphs (Fig. 7), but it is not clear when these formed.

Medium-crystalline white dolomite is developed on gray dolomite nonplanar or saddle dolomite crystals. The very coarse-crystalline white dolomite, marked by centimeter-size

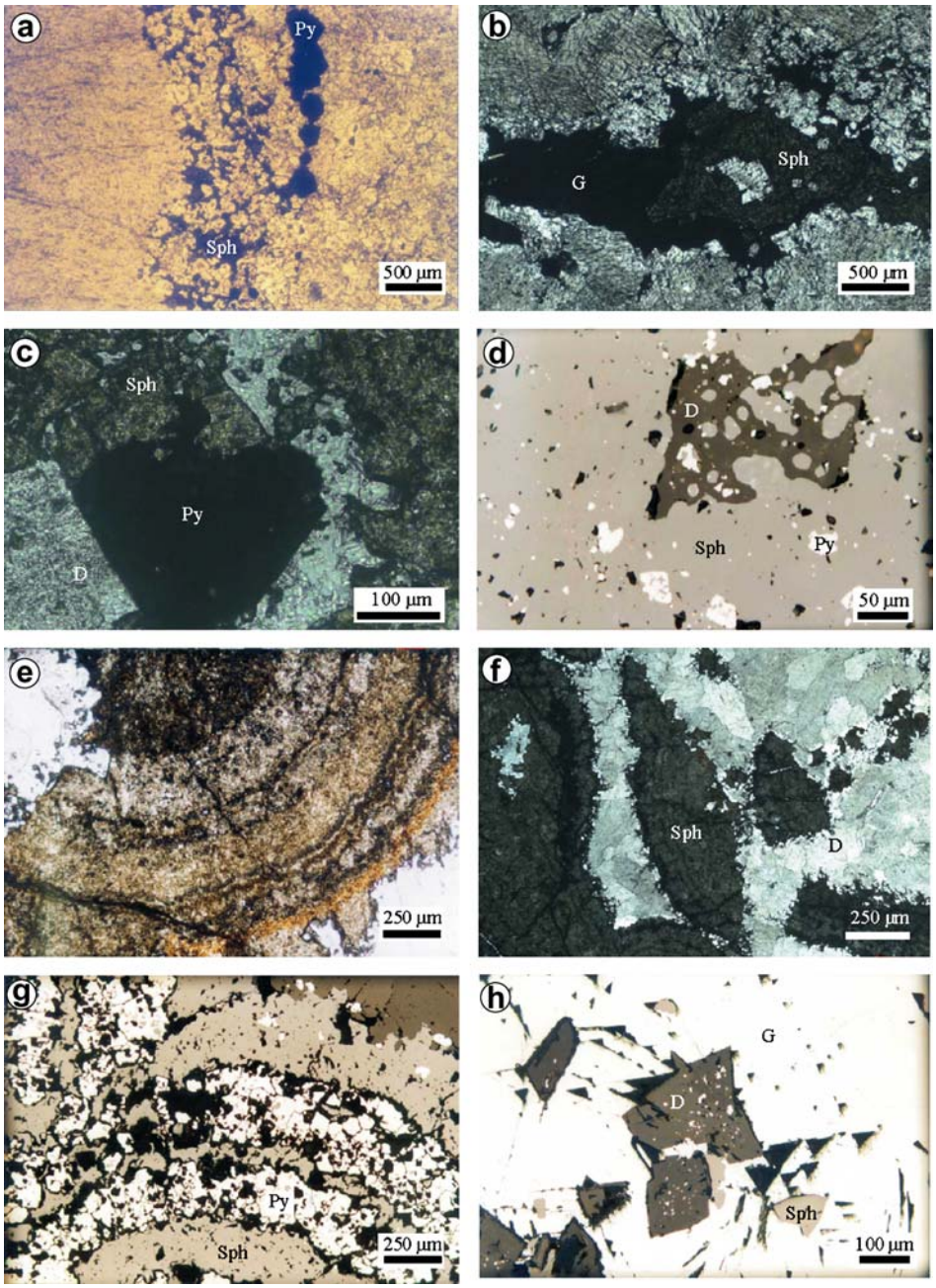

Fig. 5 Photomicrographs. **a** Transmitted light photomicrograph of host rock dolomite fragment (on the *right*) with pyrite (*Py*) and sphalerite (*Sph*) at the transition to stage III gray dolomite (on the *left*) from a brecciated Kicking Horse sample. **b** Transmitted light photomicrograph of galena (*G*) replacing sphalerite (*Sph*) in a dolomite sample from the Kicking Horse locality. **c** Transmitted light photomicrograph showing pyrite (*Py*) and dolomite (*D*), both partially replaced by sphalerite (*Sph*) in a Kicking Horse sample. **d** Incident light photomicrograph of dolomite (*D*) crystal and small pyrite crystals (*Py*), both corroded and partially replaced by sphalerite (*Sph*) from a Kicking Horse sample. **e** Transmitted light photomicrograph of stage III banded sphalerite from the Monarch locality. Dolomite is present in the *left upper* and *right lower corner*. **f** Transmitted light photomicrograph of broken stage III banded sphalerite (*Sph*) fragments cemented by stage III gray dolomite (*D*) from a Kicking Horse sample. **g** Incident light photomicrograph of alternating small colloform bands of stage III pyrite and sphalerite from the Kicking Horse sample. **h** Incident light photomicrograph of galena (*G*) with typical triangular pits and a few inclusions of sphalerite (*Sph*) and also dolomite (*D*) fragments

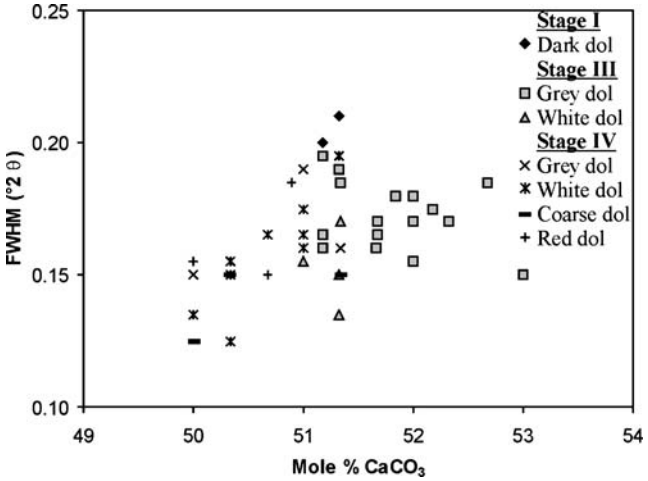

Fig. 6 Diagram of dolomite nonstoichiometry (expressed in mol.% $CaCO_3$) versus degree of ordering (FWHM, °2θ) of Kicking Horse dolomite

crystals, occurs as cement between brecciated host rock dolomite fragments. This dolomite was found associated with dolomite–pseudomorphic chlorite (identified as clinochlore by XRD analysis). Finally, the reddish dolomite has similar microscopic characteristics to the medium-crystalline white dolomite but is more intensely twinned than the other dolomite types. The reddish color may be related to alteration of the enclosed pyrite crystals.

CL-zoned calcite

The final mineral in the paragenetic sequence is transparent, CL-zoned calcite that fills fissures and has no association with sulfide mineralization. Hence, this calcite will not be further discussed.

The minerals discussed above can be grouped in different stages, based mainly on cross-cutting relationships, as presented in the paragenetic sequence of Fig. 4. Host rock dolomite is assigned to stage I, disseminated sulfide to stage II, most nondisseminated sulfide and ore-associated carbonate to stage III, late-coarse pyrite and dolomite cements from barren samples to stage IV, and late CL-zoned calcite to stage V.

Carbonate geochemistry

While all stage III and IV carbonate types from the Kicking Horse locality were analyzed geochemically, only stage III gray and stage IV white and reddish dolomite from the Monarch locality could be analyzed because of the limited number of samples of sufficient purity. Results for Fe, Mn, Na, and Sr are presented in Fig. 8. Data for both localities show clearly that Fe and Mn concentrations are very high in stage III gray dolomite (Fe=12,227–48,204 ppm; Mn=2,484–5,885 ppm). In contrast, they are rather low in stage IV reddish and coarse-crystalline white dolomite (Fe: =1,389–2,927 ppm; Mn=127–325 ppm), while the other stage III and IV dolomite has intermediate values (Fe=4,500–9,370 ppm; Mn=591 to 2,242 ppm). All dolomites are characterized by relatively low Sr and high Na concentrations. Although the Sr content does not vary significantly between different types (26–79 ppm), the stage IV reddish dolomite at the Kicking Horse locality has slightly higher Sr values (161–166 ppm). Similar to Fe and Mn, Na concentrations are highest in the stage III gray dolomite (189–308 ppm) and lowest in stage IV reddish and coarse-crystalline white dolomite (96–160 ppm), while intermediate in the other stage III and IV dolomite (142–203 ppm).

K was generally very low in the samples, with values between 13 and 31 ppm. Cu was below the detection limit in all the analyzed samples. Pb and Zn analyses gave scattered results with values varying from below the detection limit to 48 ppm (excluding two outliers) for Pb and up to 5,900 ppm for Zn.

Table 1 Cathodoluminescence (CL) characteristics of different dolomite types

Stage	Type	Mineral	Cathodoluminescence characteristics
I	Dark	Dolomite	Non to dark brownish red CL with bright orange CL patches
I	Gray	Dolomite	Non to dark brownish red CL with bright orange CL patches
III	Gray	Dolomite	Nonluminescent with sometimes yellow bright CL spots in the crystal cores
III	White	Dolomite	Nonluminescent with sometimes yellow bright CL spots in the crystal cores
III	Transparent	Calcite	Greenish yellow CL
IV	Gray	Dolomite	Nonluminescent
IV	White	Dolomite	Band of alternating non, bright and dull zonations and then, orange bright CL
IV	Coarse, white	Dolomite	Non, bright orange and dull red zonations
IV	Reddish	Dolomite	Mostly orange bright CL
V	Transparent	Calcite	Non and bright yellowish CL zonations

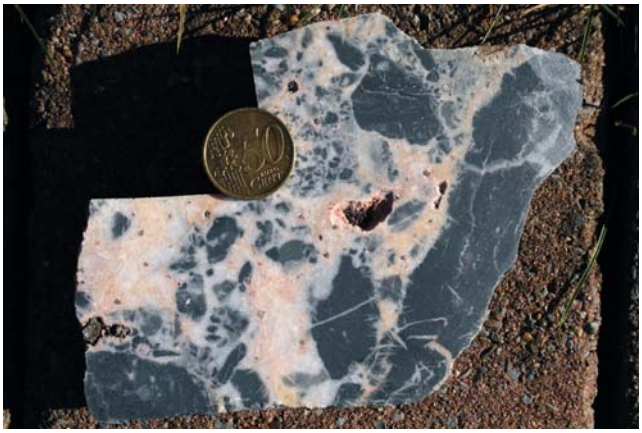

Fig. 7 Macrophotograph of breccia with different dolomite cements. Notice the presence of needlelike crystals that are interpreted as evaporite pseudomorphs (coin diameter is 2.5 cm)

Isotopic analysis

Stable oxygen and carbon isotope signatures

The $\delta^{18}O$ values of the carbonate samples (Fig. 9) vary between −20.6 and −14.3‰, and $\delta^{13}C$ values vary between −2.7 and −0.2‰ VPDB (excluding one stage I dolomite sample of $\delta^{18}O$=−11.2‰ and $\delta^{13}C$=+1.0‰ VPDB). Among the Kicking Horse samples, the $\delta^{13}C$ values differ between stage III and stage IV dolomite. Stage I and stage III carbonate have $\delta^{13}C$ values higher than −1.0‰ VPDB (one sample excluded), whereas $\delta^{13}C$ values of stage IV dolomite fall between −2.4 and −1.0‰ VPDB. In contrast, the Monarch samples do not display a comparable $\delta^{13}C$ difference. Although stage IV dolomite has similar $\delta^{13}C$ values (−2.7 to −1.3‰ VPDB) as at the Kicking Horse locality, the $\delta^{13}C$ values of older carbonate types are not distinctly higher at the Monarch locality. At the latter locality, the $\delta^{18}O$ values are generally higher for stage I and stage III carbonate compared to stage IV dolomite. Among the Kicking Horse samples, the average $\delta^{18}O$ value of stage IV dolomite is lower than the average $\delta^{18}O$ value of stage I and stage III carbonate. In the stage IV dolomite, the lowest $\delta^{13}C$ and $\delta^{18}O$ values are found in reddish and coarse-crystalline white dolomite.

Sr isotope ratios

Most of the $^{87}Sr/^{86}Sr$ values lie between 0.7087 and 0.7123; only two samples from the Monarch locality exceed this range, with values of 0.7147 and 0.7162 (Fig. 10). While there is a clear decrease in $^{87}Sr/^{86}Sr$ ratios in the younger carbonate types in the Kicking Horse samples, the Monarch dolomite has a rather scattered, erratic pattern. In the Kicking Horse samples, higher $^{87}Sr/^{86}Sr$ values are measured in stage III carbonate (0.7115–0.7123) compared to stage IV dolomite (0.7087–0.7112), where the reddish and coarsely crystalline white dolomite have the lowest ratios. $^{87}Sr/^{86}Sr$ values correlate well with $\delta^{18}O$ values. Among the Monarch samples, stage III gray dolomite also has the highest $^{87}Sr/^{86}Sr$ (0.7162), but stage III white dolomite is characterized by the lowest $^{87}Sr/^{86}Sr$ (0.7106). Furthermore, stage IV reddish dolomite has the highest $^{87}Sr/^{86}Sr$ (0.7111–0.7147) compared to 0.7108–0.7111 for the other measured stage IV samples.

Fluid inclusion analysis

Microthermometry

Microthermometric analysis was performed on fluid inclusions in quartz, sphalerite, dolomite, and calcite. The fluid inclusions were classified petrographically as being primary, pseudosecondary, and secondary based on their relation to growth zones according to the criteria of Roedder (1984). Those that are labeled as "not certain" have characteristics similar to the primary and pseudosecondary inclusions but could not be confidently assigned to either category. In calcite, at 20°C, most fluid inclusions contain a single-phase aqueous liquid and are up to 10×5 μm in size. The rare two-phase inclusions observed in the calcite are 5×3 μm in size. Most fluid inclusions in the other minerals contain two phases (L+V) at 20°C and are up to 9×3 μm in size in quartz or less than 4×2 μm in dolomite. The microthermometric study of fluid inclusions hosted by sphalerite was hampered by the small number of visible fluid inclusions, the fact that most fluid inclusions in coarse-crystalline sphalerite occur in secondary trails, and because of the optical characteristics of the inclusions in the host mineral (the inclusions have a dark appearance). Nevertheless, small (generally less than 3×2 μm) two-phase fluid inclusions trapped in primary growth bands could be identified (Fig. 11) and were analyzed.

The first visible melting of the frozen fluid inclusions in the different minerals occurred at approximately −52°C. Only the secondary fluid inclusions recognized in stage IV reddish dolomite from the Kicking Horse locality are characterized by a first melting temperature of about −22°C. The melting of hydrohalite was generally observed to occur before the melting of ice and at temperatures of around −30°C; however, the small size of the fluid inclusions prevented an accurate temperature measurement of this phase change.

Both the homogenization temperatures and the final ice melting temperatures, measured in fluid inclusions in different minerals from both study localities, are presented in Table 2. The data show that primary fluid inclusions in sphalerite (66–99°C) and quartz (63–99°C) have lower homogenization temperatures than those in dolomite (95–167°C). The final ice-melting temperatures in dolomite are similar or

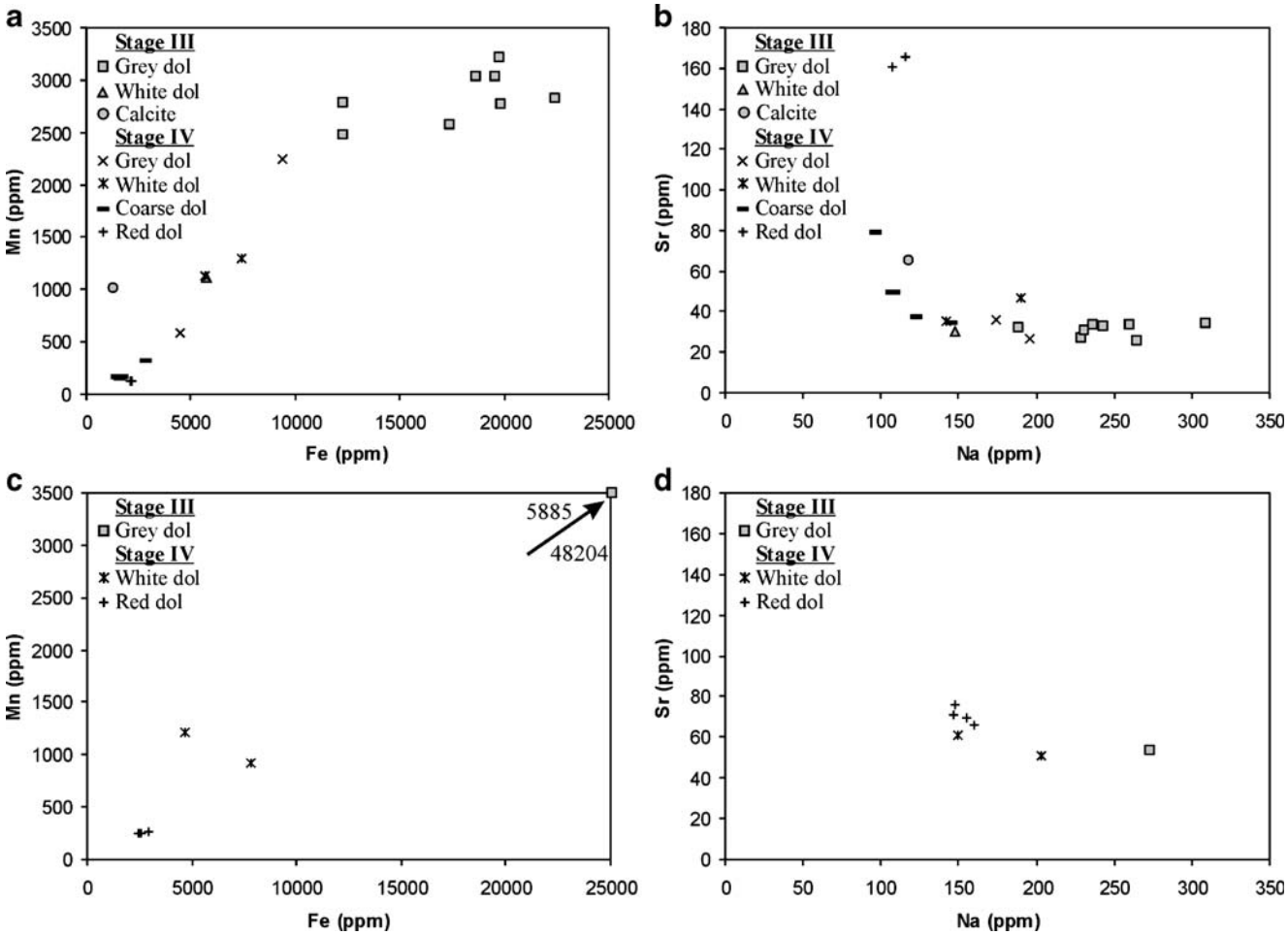

Fig. 8 Carbonate geochemistry plots. Respectively, Fe versus Mn and Na versus Sr diagram of **a, b** Kicking Horse and **c, d** Monarch carbonate

lower than those in sphalerite but higher than those in quartz. The Tm_{ice} values can be used in the equation of Bodnar (1993) to calculate the fluid salinity (as melting of hydrohalite occurs before melting of ice), which varies from 20.3 to 30.2 wt% NaCl eq. Sphalerite is characterized by the lowest average salinity (23 wt% NaCl eq.) measured in primary fluid inclusions at both mines, whereas quartz (from the Kicking Horse Mine) has the highest average salinity (28 wt% NaCl eq.) compared to dolomite (Fig. 12). Different from the other minerals, fluid inclusions (of which the origin could not be confidently determined) in stage III calcite have lower homogenization temperatures (50–72°C) and a lower salinity (17.4–21.7 wt% NaCl eq).

As shown by the data in Table 2, the homogenization and ice-melting temperatures are similar for primary, pseudosecondary, and fluid inclusions of uncertain origin in most minerals.

Crush–leach geochemistry

The raw leachate data and the molar element ratios of inclusion fluids in different mineral types from the Kicking Horse and Monarch localities are presented in Tables 3 and 4. While the Br concentration is below the detection limit (0.005 ppm) in stage III sphalerite ($n=1$) and galena ($n=1$) samples, higher concentrations were determined for stage III quartz, pyrite, and stage III and IV carbonate. Cl/Br molar ratios for leachates of this group vary from 285 to 697 with the lowest value represented by calcite and the highest values by quartz and stage IV coarse white dolomite (Fig. 13a,b). Na/Br molar ratios are generally higher for Monarch dolomite than Kicking Horse dolomite (Fig. 13a,b). Li/Na molar ratios are generally higher in stage III than in the stage IV dolomite (Fig. 13c,d). For quartz, the Ca, K, and Mg contents were also determined; the molar Ca/Na ratio is 0.34, and the molar K/Na and Mg/Na ratio are both 0.14.

Discussion

General characteristics of the deposits

The Kicking Horse and Monarch ore deposits both have a simple sulfide mineralogy consisting of pyrite, sphalerite, and

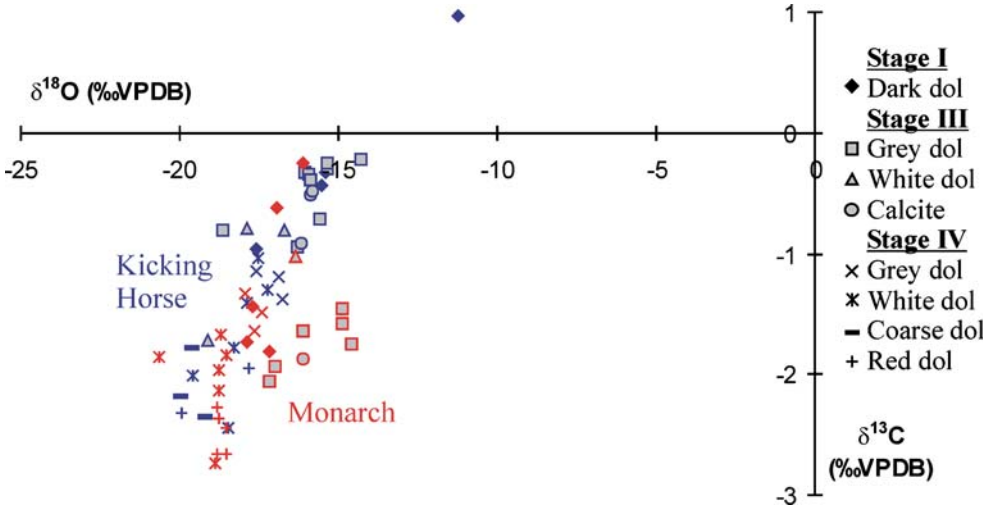

Fig. 9 Cross-plot of stable isotopic compositions from Kicking Horse (*in blue*) and Monarch (*in red*) carbonate

galena. Ore formation was accompanied by significant dolomitization and also small amounts of quartz, sericite, and calcite were precipitated in the mineralizing system. The sulfide mineralogy, carbonate environment, and structural setting are consistent with the characteristics of MVT ore deposits (e.g., Sverjensky 1986). Moreover, the deposits are stratigraphically controlled, being restricted to the Middle Cambrian Cathedral Formation.

Although the sulfide mineralogy is simple, a variety of different mineral stages, types, and textures were distinguished and have been presented here for the first time. Previous, now quite dated, mineralogical descriptions of earlier studies are less detailed compared to more current techniques. Goranson (1937) had recognized already two forms of white dolomite in these units, one preceding sulfide mineralization and a second later dolomite containing "pyritohedrons." Sulfide occurs as disseminations in the host rock, individual grains, coarsely crystalline overgrowths on brecciated clasts, in the center of carbonate cements, and as alternating sulfide bands displaying colloform textures. Pyrite can occur as euhedral cubes, which is typical of this mineral (Craig and Vaughan 1990). Some of the sulfide, such as the disseminated forms (stage II sulfide), replaces dolomite, whereas the coarse-crystalline types, such as inclusion-poor stage III sphalerite and galena, are open-space fillings. Although the disseminated sulfide is interpreted to occur at an earlier stage than the coarse-crystalline sulfide, we cannot completely exclude the possibility that these were contemporaneous.

Dolomite is characterized by a relatively good stoichiometry, with a rough correlation between $CaCO_3$ mol% and Fe content. Stage III gray dolomite shows the largest stoichiometric deviation, which is caused by their high Fe content. This can be explained by the fact that Ca in the $CaMg(CO_3)_2$ structure is substituted by Fe. Hence, based on the relationship between d_{104} spacing and $FeCO_3$ content of dolomite (Al-Hashimi and Hemingway 1974), an Fe content of up to 4.8% would decrease the mole percent of $CaCO_3$ by up to about 1.7 in this carbonate. Consequently, all dolomite types are nearly stoichiometric.

Several types of dolomite cements are associated with brecciation events. Although the breccias are not the topic of this study, we could suggest that the breccias from stage III may result from hydrothermal dissolution collapse based on the texture of the infill carbonate material between the fragments, unless the samples contained depositional clasts that form part of a storm bed. The breccias from stage IV likely had a tectonic origin. However, a stratigraphic mechanism, such as evaporite dissolution, cannot be excluded for the latter.

Origin and type of mineralizing fluids

Composition and salinity of fluids

The fluid inclusion data from the sphalerite, associated dolomite and quartz from the Kicking Horse and Monarch localities, suggest the minerals precipitated from highly saline H_2O–NaCl–$CaCl_2$(–KCl–$MgCl_2$) fluids. This fluid composition was deduced from fluid inclusion first melting temperatures (of about −52°C) and bulk crush–leach analysis. The crush–leach dataset from quartz demonstrates that the fluids have a molar Na-to-Ca ratio of 2.9, Na-to-K ratio of 7.1, and Na-to-Mg ratio of 7.0, implying that the fluids contain 5.0% Na, 3.0% Ca, 1.2% K, and 0.7% Mg (back-calculated using the salinity data). The molar Na/Mg ratio is very similar, and the Na/Ca ratio is slightly lower than the ratios reported by Yang et al. (1995) for fluid inclusion waters in dolomite from the Cambrian Cathedral Formation in Western Canada. In general, the molar Cl/Na, Cl/K, and K/Na ratios in the dolomite-hosted inclusion fluids are similar to those found in the studies of Yang et al. (1995); Nesbitt and Prochaska (1998); and Vandeginste et al. (2005)

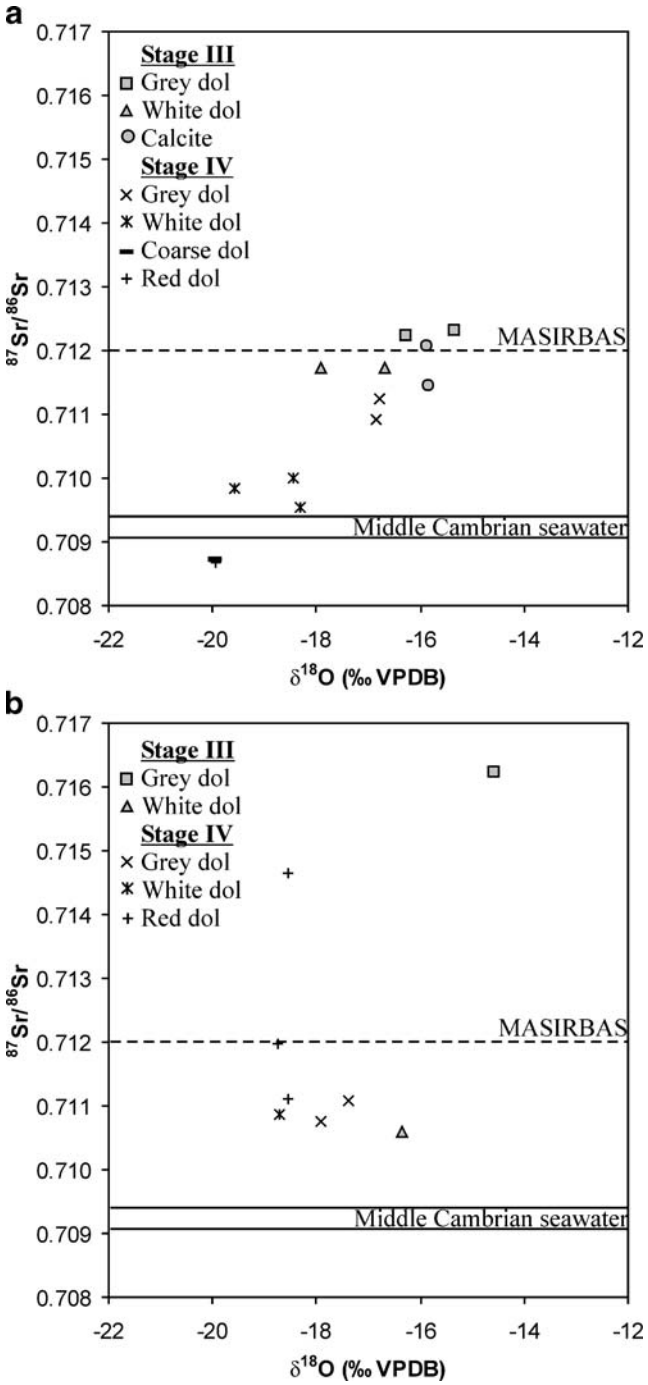

Fig. 10 $^{87}Sr/^{86}Sr$ values represented on a plot versus $\delta^{18}O$ values of **a** Kicking Horse and **b** Monarch carbonate. The signature of Middle Cambrian seawater (Veizer et al. 1999) and the MASIRBAS value (maximum Sr isotope ratio of basinal shale in the Western Canada Sedimentary Basin as defined by Machel and Cavell 1999) are also indicated

for dolomite in the Middle Cambrian formations of Western Canada (Fig. 14). We also note that the K/Na ratios are similar in both sulfide and dolomite samples. This suggests that residual solid inclusions retained during any dissolution and precipitation reactions during sulfide formation are not modifying this ratio to any great extent. Thus, we believe the K/Na ratio is representative of the mineralizing fluids.

The fluid salinities (20.3 to 30.2 wt% NaCl eq.) fall within the range typical of MVT ore-forming fluids namely, ~16–26 wt% $CaCl_2$ eq. (e.g., Basuki and Spooner 2004), and are similar to the values reported by Nesbitt and Muehlenbachs (1994) for dolomite from the Kicking Horse and Monarch localities. Our results are similar to reported fluid inclusion salinity data from Paleozoic dolomite in the Western Canada Sedimentary Basin (e.g., Aulstead et al. 1988; Mountjoy and Halim-Dihardja 1991; Mountjoy et al. 1999; Qing and Mountjoy 1994; Vandeginste et al. 2005; Wendte et al. 1998; Yao and Demicco 1995, 1997).

Origin and evolution of fluids on flow path

The halogens Cl and Br often behave conservatively in solution and are relatively unaffected by most fluid–rock interactions; thus, they are commonly used to distinguish between the origin of different fluids (e.g., Carpenter 1978; Kharaka et al. 1987; Rittenhouse 1967). In contrast to the halogens, the cation contents of fluids are strongly modified by fluid–rock interactions (e.g., Boiron et al. 1996). On the basis of halogen compositions of the fluid inclusion leachates, three main types of fluids can be distinguished in this study namely, fluid 1 found in dolomite, quartz, and pyrite, fluid 2 in calcite, and fluid 3 present in sphalerite and galena. However, we note that the existence of fluid 2 is based on one sample and fluid 3 on two samples; consequently, the interpretations presented are tentative.

Fluid 1 The molar Cl/Br and Na/Br ratios from most dolomite, quartz, and pyrite are lower than values for seawater (except for the Cl/Br of one Kicking Horse stage IV coarse-crystalline white dolomite sample and Na/Br of one

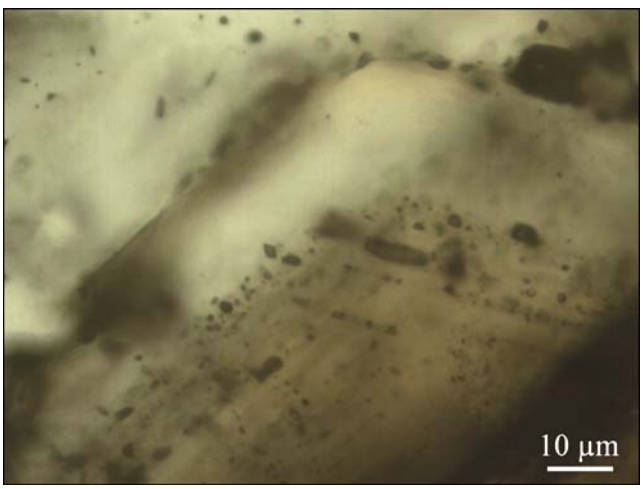

Fig. 11 Microphotograph of fluid inclusions in growth zones in stage III sphalerite from the Monarch locality

Table 2 Homogenization (Th) and final ice melting (Tm_{ice}) temperature data of fluid inclusions in different mineral types from the Kicking Horse and Monarch localities

Location	Host mineral	Inclusion origin	Tm_{ice} (°C)			Th (°C)		
			Range	Mean	Number	Range	Mean	Number
Kicking Horse	III sphalerite	Primary	−26.4 to −17.1	−21.5	24	68 to 92	86	24
Kicking Horse	III sphalerite	Pseudosecondary			0	93		1
Kicking Horse	III sphalerite	Not certain	−20.6		1	75 to 93	80	4
Kicking Horse	III quartz	Primary	−32.4 to −25.0	−28.9	10	63 to 99	81	31
Kicking Horse	III quartz	Not certain	−31.5 to −22.2	−27.2	8	62 to 95	75	15
Kicking Horse	III gray dolomite	Primary	−27.3 to −21.5	−23.3	21	117 to 150	133	33
Kicking Horse	III gray dolomite	Not certain	−24.2 to −18.6	−21.4	6	111 to 134	123	19
Kicking Horse	III calcite	Not certain	−19.0 to −13.9	−16.3	11	50 to 72	65	9
Kicking Horse	IV gray dolomite	Primary	−25.4 to −17.7	−21.3	25	105 to 133	118	32
Kicking Horse	IV gray dolomite	Not certain	−24.1 to −19.6	−22.4	12	101 to 151	132	22
Kicking Horse	IV white dolomite	Primary	−29.7 to −18.4	−23.0	23	121 to 167	144	45
Kicking Horse	IV white dolomite	Pseudosecondary			0	159 to 160	160	2
Kicking Horse	IV white dolomite	Not certain	−27.1 to −17.2	−21.9	17	115 to 166	141	15
Kicking Horse	IV coarse dolomite	Primary	−30.5 to −17.4	−24.7	21	106 to 152	132	32
Kicking Horse	IV coarse dolomite	Pseudosecondary	−25.1 to −19.3	−23.0	3			0
Kicking Horse	IV coarse dolomite	Not certain	−23.6 to −18.1	−21.5	8	111 to 123	117	3
Kicking Horse	IV reddish dolomite	Primary	−28.6 to −22.9	−24.5	11	103 to 143	128	17
Kicking Horse	IV reddish dolomite	Pseudosecondary			0	156 to 159	158	4
Kicking Horse	IV reddish dolomite	Secondary	−11.4 to −7.7	−9.1	4	136 to 152	143	3
Kicking Horse	IV reddish dolomite	Not certain	−25.7 to −21.6	−24.1	14	118 to 174	146	14
Monarch	III sphalerite	Primary	−24.8 to −18.6	−21.4	19	66 to 99	80	24
Monarch	III sphalerite	Pseudosecondary	−23.2 to −21.8	−22.5	2	73 to 109	92	5
Monarch	III sphalerite	Not certain	−20.7		1	74 to 91	85	3
Monarch	III gray dolomite	Primary	−25.7 to −17.3	−21.7	22	99 to 141	119	34
Monarch	III gray dolomite	Not certain	−24.8 to −20.1	−22.7	12	103 to 146	131	18
Monarch	III white dolomite	Primary	−29.0 to −18.5	−24.4	24	110 to 142	124	29
Monarch	III white dolomite	Pseudosecondary	−23.8 to −21.7	−22.8	2	122 to 138	131	3
Monarch	III white dolomite	Not certain	−28.3 to −19.1	−24.7	6	94 to 130	111	10
Monarch	IV gray dolomite	Primary	−26.7 to −22.7	−24.4	15	95 to 131	110	19
Monarch	IV gray dolomite	Pseudosecondary	−26.1 to −24.7	−25.5	3	93 to 99	95	5
Monarch	IV gray dolomite	Secondary			0	123 to 131	127	3
Monarch	IV gray dolomite	Not certain	−27.1 to −19.0	−21.9	12	105 to 127	115	18
Monarch	IV white dolomite	Primary	−29.9 to −21.5	−24.9	19	95 to 128	107	26
Monarch	IV white dolomite	Not certain	−27.2 to −22.8	−24.7	7	96 to 137	118	10
Monarch	IV reddish dolomite	Primary	−29.1 to −23.1	−25.7	14	142 to 157	151	13
Monarch	IV reddish dolomite	Pseudosecondary	−24.7		1	170 to 177	173	4
Monarch	IV reddish dolomite	Not certain	−27.1 to −17.7	−24.1	21	128 to 193	164	5

The data range, mean value and the number of measurements are given.

Monarch stage III gray dolomite sample; Fig. 13a,b), suggests that the mineralizing brines obtained their salinity by the evaporation of seawater. The reported molar Cl/Br ratios are higher in this study (302–697) than those reported by Nesbitt and Prochaska (1998) for dolomite (184–222) from the Kicking Horse and Monarch MVT mineralization. However, these data were likewise interpreted by Nesbitt and Prochaska (1998) to indicate the mineralizing fluids formed from evaporated seawater.

Chi and Savard (1997) noted that a similar distribution of data on these ratio plots can be the result of mixing. To assess whether this may be an issue in this study, absolute Cl and Br concentrations in dolomite- and quartz-hosted fluid inclusions were calculated using the salinity data acquired from microthermometry. The reconstructed halogen compositions of the fluids confirm that the salinity of the brines originated from the evaporative concentration of seawater (Fig. 13e,f). In this figure, it can also be seen that although the stage III gray dolomite and stage IV coarse dolomite samples plot on the Seawater Evaporation Trajectory (SET) before the point of halite precipitation, the other samples lie below the SET curve past the point of halite precipitation (Fig. 13e,f). The departure of the data from the SET can be explained by mixing of a halite saturated brine with

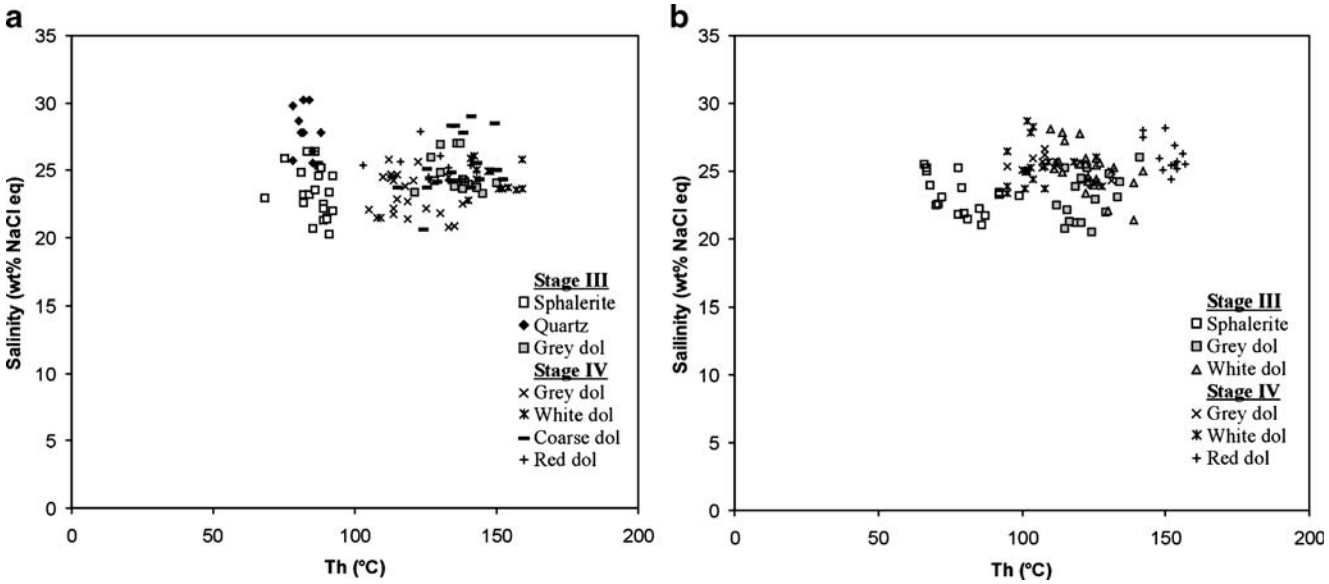

Fig. 12 Overview of the microthermometric data, presented in a homogenization temperature (*Th*) versus salinity plot, from primary fluid inclusions in different mineral types from the **a** Kicking Horse and **b** Monarch locality

Table 3 Leachate data for each analyzed sample from the Kicking Horse and Monarch locality (data in ppm)

Location	Mineral type	Sample	IC				AAS			Charge
			Cl	Br	F	SO_4	Na	K	Li	balance
Kicking Horse	III pyrite	CN02VV164	37.27	0.21	<0.001	<0.001	7.11	0.89	0.005	0.21
Kicking Horse	III sphalerite	CN03VV059	4.41	<0.005	<0.001	0.46	10.26	0.56	<0.001	2.22
Kicking Horse	III galena	CN03VV060	2.67	<0.005	0.51	0.90	2.42	0.01	<0.001	0.59
Kicking Horse	III quartz	CN03VV053a	33.72	0.13	<0.001	0.23	10.04	0.12	0.006	0.30
Kicking Horse	III gray dolomite	CN02VV153	35.10	0.22	<0.001	0.94	13.18	1.42	0.007	0.40
Kicking Horse	III gray dolomite	CN02VV152a	28.64	0.16	0.02	0.84	11.30	1.09	0.008	0.42
Kicking Horse	III gray dolomite	CN03VV055	57.48	0.32	<0.001	0.48	17.89	1.78	0.019	0.34
Kicking Horse	III gray dolomite	CN03VV026	41.60	0.24	<0.001	0.16	13.36	1.22	0.018	0.35
Kicking Horse	III gray dolomite	CN03VV046a	–	–	–	–	16.32	1.78	0.019	
Kicking Horse	III gray dolomite	CN03VV054	33.34	0.20	0.22	0.1	13.15	1.15	0.013	0.42
Kicking Horse	III gray dolomite	CN03VV053b	48.28	0.36	<0.001	<0.001	12.03	0.91	0.010	0.27
Kicking Horse	III white dolomite	CN03VV057a	19.46	0.12	<0.001	0.24	8.24	0.50	<0.001	0.44
Kicking Horse	III calcite	CN03VV046b	45.66	0.36	0.06	0.18	9.98	1.01	0.018	0.24
Kicking Horse	IV gray dolomite	CN03VV048	19.86	0.09	<0.001	3.22	9.11	0.76	0.007	0.43
Kicking Horse	IV gray dolomite	CN03VV057b	62.30	0.36	<0.001	0.14	10.90	0.84	0.005	0.19
Kicking Horse	IV white dolomite	CN02VV152b	9.06	0.05	<0.001	0.08	4.74	0.35	0.001	0.55
Kicking Horse	IV white dolomite	CN03VV057c	28.75	0.12	<0.001	<0.001	7.18	0.39	0.004	0.26
Kicking Horse	IV coarse, white dolomite	CN02VV156	13.51	0.06	<0.001	0.64	6.28	0.38	0.001	0.47
Kicking Horse	IV coarse, white dolomite	CN02VV158	37.14	0.12	<0.001	2.82	13.38	1.15	<0.001	0.36
Kicking Horse	IV reddish dolomite	CN03VV036	7.35	0.04	<0.001	1.27	5.25	0.37	0.001	0.65
Monarch	III gray dolomite	CN04VV147	55.56	0.20	<0.001	0.28	33.16	2.50	0.044	0.64
Monarch	IV gray dolomite	CN04VV137a	40.15	0.19	<0.001	1.30	28.31	4.26	0.006	0.78
Monarch	IV white dolomite	CN04VV158	43.92	0.24	<0.001	0.47	27.14	2.01	0.009	0.65
Monarch	IV white dolomite	CN04VV137b	60.97	0.35	<0.001	1.50	–	1.83	0.007	
Monarch	IV reddish dolomite	CN04VV136a	30.60	0.14	<0.001	2.37	22.04	1.51	0.018	0.71
Monarch	IV reddish dolomite	CN04VV136b	33.84	0.17	0.10	9.73	22.84	1.25	0.022	0.55
Monarch	IV reddish dolomite	CN04VV144	37.99	0.18	0.17	3.36	–	1.58	0.045	

Table 4 Crush–leach molar ratio data of inclusion fluids in different mineral types from the Kicking Horse and Monarch locality

Location	Mineral type	n	Cl/Br (molar)	Na/Br (molar)	K/Br (molar)	Li/Na (molar)	K/Na (molar)	Ca/Na (molar)	Mg/Na (molar)
Kicking Horse	III pyrite	1	399	118	8.64	0.0022	0.0735	–	–
Kicking Horse	III sphalerite	1	>1984	>7132	>228.89	<0.0003	0.0321	–	–
Kicking Horse	III galena	1	>1202	>1682	>2.45	<0.0014	0.0015	–	–
Kicking Horse	III quartz	1	584	268	1.89	0.0020	0.1411	0.3442	0.1419
Kicking Horse	III gray dolomite	7	302–404	116–246	5.18–13.95	0.0018–0.0045	0.0446–0.0640	–	–
Kicking Horse	III white dolomite	1	365	239	8.58	<0.0004	0.0360	–	–
Kicking Horse	III calcite	1	285	96	5.72	0.0060	0.0594	–	–
Kicking Horse	IV gray dolomite	2	389–497	105–352	4.77–17.17	0.0015–0.0026	0.0453–0.0488	–	–
Kicking Horse	IV white dolomite	2	408–539	208–330	6.68–14.22	0.0008–0.0019	0.0321–0.0431	–	–
Kicking Horse	IV coarse, white dolomite	2	507–697	364–388	13.08–19.62	<0.0002–0.0006	0.0359–0.0506	–	–
Kicking Horse	IV reddish dolomite	1	414	456	19.01	0.0008	0.0417	–	–
Monarch	III gray dolomite	1	641	591	26.24	0.0044	0.0444	–	–
Monarch	IV gray dolomite	1	488	532	47.02	0.0007	0.0884	–	–
Monarch	IV white dolomite	2	391–412	393	10.68–17.12	0.0011	0.0436	–	–
Monarch	IV reddish dolomite	3	453–499	473–555	15.21–22.30	0.0027–0.0032	0.0322–0.0402	–	–

For measurements of Br and Li that were below the detection limit, ratios were calculated using <0.005 ppm for Br and <0.001 ppm for Li.

approximately 20% of a Cl-poor fluid (e.g., Connolly et al. 1990).

Molar Na/Br ratios for dolomite, quartz, and pyrite leachates vary between 105 and 591, which is generally higher than those for the studied MVT mineralization-related dolomite for this area reported in the literature at 135–169 (Nesbitt and Prochaska 1998).

While molar Li/Na ratios in the Kicking Horse stage IV coarse-crystalline white dolomite are similar to ratios measured in Upper Devonian to Lower Cretaceous formation waters in the Alberta Basin (Connolly et al. 1990), the majority of the leachates hosted by other mineral types have higher Li/Na ratios at both localities, with the highest values occurring in stage III gray dolomite. These values are significantly higher than the values expected from an evaporated seawater and may suggest the fluids have interacted and acquired Li from units containing Li-bearing clays or with the crystalline basement (Banks et al. 2002).

Fluid 2 The molar Cl/Br and Na/Br ratios from a single sample of the ore-associated calcite suggest the fluids that formed this phase are brines that are derived from the evaporation of seawater (Fig. 13a). This is confirmed by the absolute Cl and Br concentrations calculated from the microthermometric salinity data (Fig. 13e), suggesting mixing with approximately 30% of a dilute fluid based on the departure from the SET (Connolly et al. 1990).

The calcite leachate shows a similar cation distribution to that from dolomite, quartz, and pyrite, but it is characterized by the highest molar Li/Na ratio (0.006).

Fluid 3 A fluid of quite different composition was found in the sphalerite and galena leachates. In these, Br was below the detection limit of the ion chromatograph. If we consider a detection limit of 0.005 ppm, then the molar Cl/Br and Na/Br ratios in these leachates must be greater than 1,984 and 7,132 in sphalerite and 1,202 and 1,682 in galena. These values are much higher than those found in modern-day seawater or evaporated seawater, and as a result, it can be interpreted that halite dissolution contributed to the salinity in these samples (Kesler et al. 1996). There are no microthermometric data available for the galena, but for the sphalerite sample, the average salinity can be used to back-calculate the absolute Cl and (maximum) Br concentrations to refine this interpretation. The resultant value plots to the left (log Br=2.21) of the SET curve consistent with a halite dissolution-derived fluid component (Fig. 13e).

The molar Na/Cl ratio is significantly higher in sphalerite (3.59) and galena (1.40) compared to the other mineral types (0.27–1.11). In these sulfide types, Li was below the detection limit, but assuming a maximum value of 0.001 ppm, the molar Li/Na could be up to 0.0014.

Difference between the Kicking Horse and Monarch locality

The Na/Cl ratio is generally higher and more homogeneous in Monarch samples (0.92–1.11) than in Kicking Horse samples (0.27–1.10), if we consider only the dolomite-hosted leachates. The difference between the two localities is highlighted by the K_{excess}-versus-$Na_{deficit}$ plot (Fig. 15a,b),

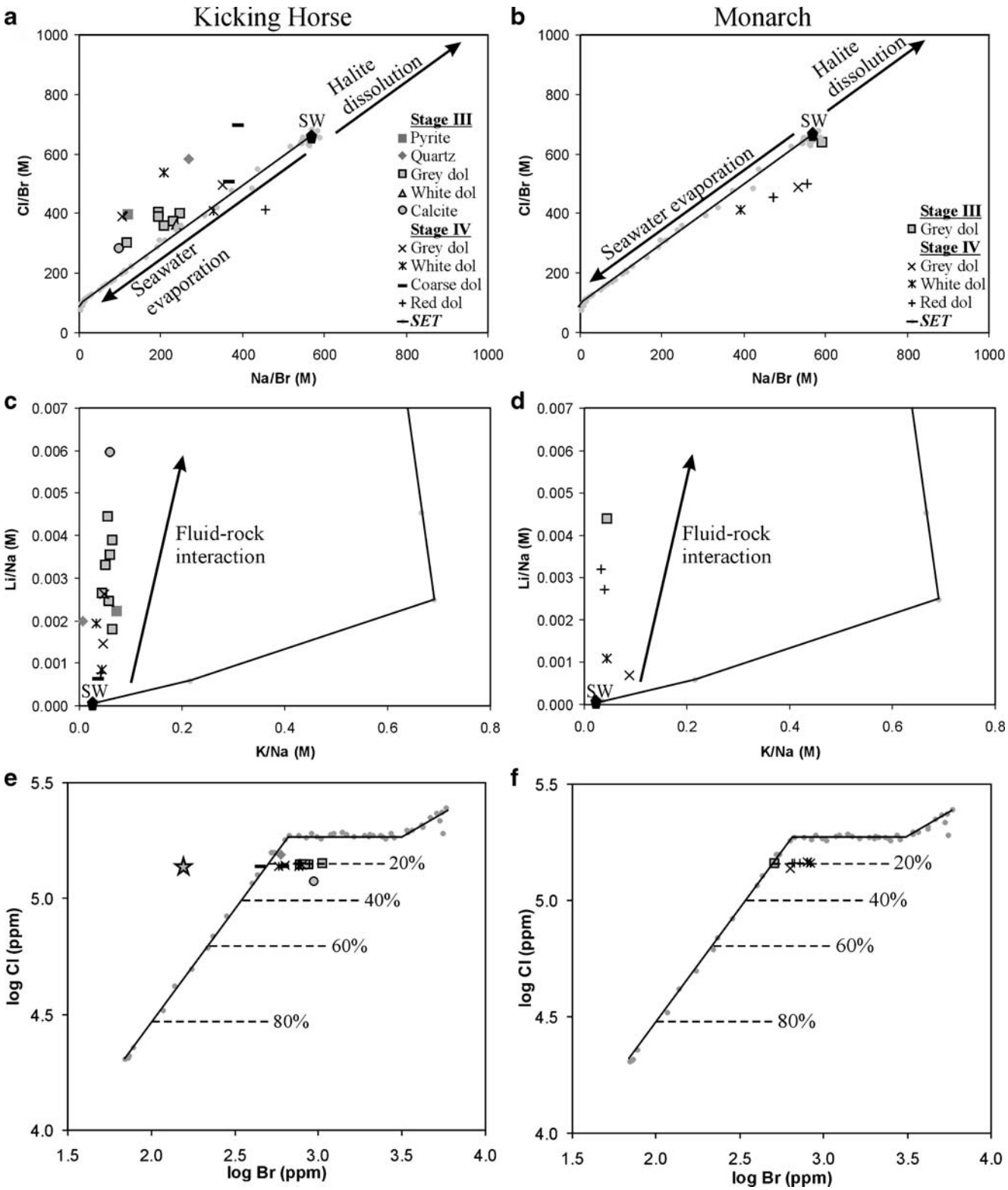

Fig. 13 Fluid inclusion crush–leach plots. **a, b** Kesler plot representing molar Na/Br versus Cl/Br ratios from the Kicking Horse and the Monarch samples, respectively. **c, d** Plot of molar K/Na versus Li/Na ratios from Kicking Horse and Monarch samples, respectively. **e, f** Log–log plot of Br versus Cl of calculated absolute concentrations based on crush–leach data in fluid inclusions from Kicking Horse and Monarch samples, respectively. *Dashed lines* represent percentage of mixing (Connolly et al. 1990). The *star* represents the calculated sphalerite data from the Kicking Horse locality using the detection limit value for Br

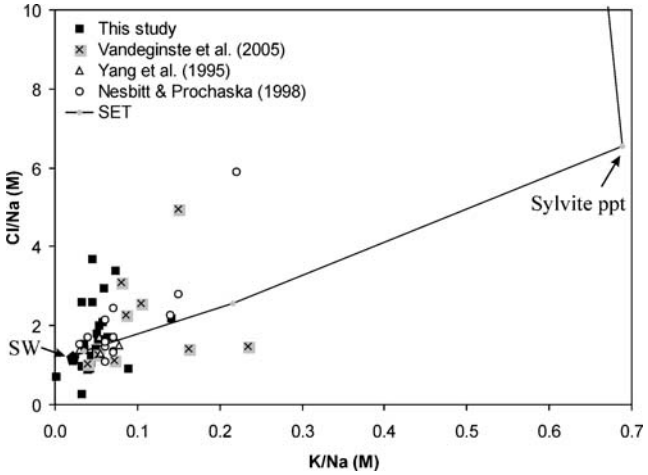

Fig. 14 Plot of leachate molar K/Na versus Cl/Na ratios from this study compared with published data on dolomite in Middle Cambrian layers in the Western Canada Sedimentary Basin close to the study area

where (except for one Kicking Horse stage IV reddish dolomite sample) all the Kicking Horse samples have a positive $Na_{deficit}$ value, whereas this value is negative for all Monarch samples. Although the differences in K_{excess} are small, there is a negative correlation between K_{excess} and $Na_{deficit}$. This implies that fluids range from more enriched in K and Na at the Monarch locality toward lower values of both cations at the Kicking Horse locality. The enrichment in K and Na might be caused by dissolution of K and Na feldspars, which may suggest that the fluids have interacted with feldspathic sandstones, such as those from the underlying Lower Cambrian Gog Group. The generally lower concentration of K at the Kicking Horse locality compared to the Monarch locality may be the result of the precipitation of the small amounts of sericite that were observed in the petrographic study. Because none of the samples were collected in situ, the possibility exists that these variations may reflect the sampling strategy. However, we did collect samples from both sites that have textures that correspond to those described from the ore zones by Ney (1954), and thus it is likely that the variations seen in the data from the two sites are real.

Temperature of fluids

Primary fluid inclusions in the ore, associated dolomite and quartz, have homogenization temperatures of 63–182°C. The low $\delta^{18}O$ values and stoichiometric nature of dolomite at the Kicking Horse and the Monarch localities support mineralization temperatures higher than 63°C. These temperatures are also typical of MVT ore-forming fluids, which are ~75–150°C (e.g., Basuki and Spooner 2004). The fluid inclusion temperatures in dolomite are similar to the range of 120–200°C reported by Nesbitt and Muehlenbachs (1994) for sparry dolomite from the Kicking Horse and Monarch localities.

There are no large variations in average homogenization temperatures in the different dolomite types. Nevertheless, primary fluid inclusions in sphalerite and quartz yield lower homogenization temperatures than those measured in dolomite (Fig. 12). In addition, stage IV reddish dolomite from the Monarch locality varies slightly toward higher temperatures, which may be caused by post-trapping effects related to an observed higher deformation degree (e.g., thicker twinning planes compared to other dolomite types).

The predominance of single-phase fluid inclusions in calcite indicates either metastability or low formation temperatures because stable single-phase fluid inclusions form at temperatures around or below 50°C (Goldstein 2001).

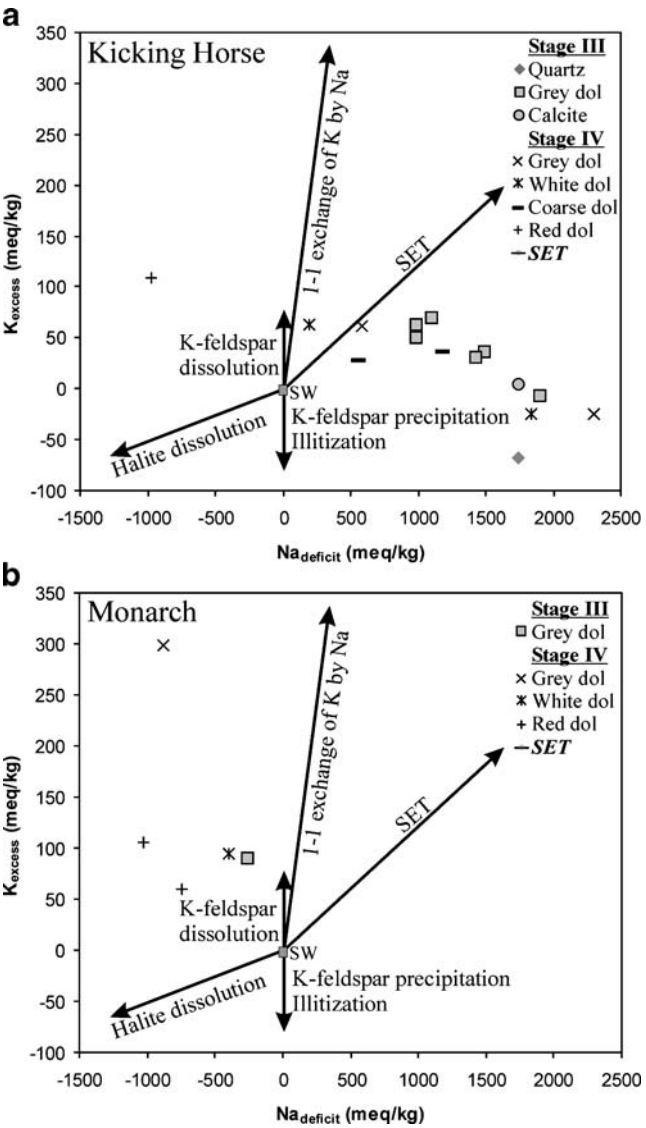

Fig. 15 K_{excess} versus $Na_{deficit}$ plot of crush–leach data in fluid inclusions (after Heijlen et al. 2001) from **a** Kicking Horse and **b** Monarch samples

Dolomite geochemistry

Several geochemical parameters exhibit a roughly linear trend from stage III gray dolomite toward stage IV reddish and coarse-crystalline white dolomite. In particular, this is observed for Fe, Mn, and Na contents, which decrease from stage III gray dolomite toward the younger stage IV dolomite (Fig. 8). Hence, the dolomite type with the highest Fe, Mn, and Na concentrations (stage III gray dolomite) is that most closely related to the main ore stage (stage III). In contrast, the Sr concentration is rather similar in all the dolomite types, except for the Kicking Horse stage IV reddish dolomite, which has slightly higher concentrations. The elemental contents could reflect a progressive buffering effect of the carbonate environment when the main sulfide precipitation comes to an end, as the metal concentration depends on both chloride content and on pH and reduced sulfur content (Plumlee et al. 1994).

A similar trend is also indicated by the $\delta^{18}O$–$\delta^{13}C$ values of carbonate at the Kicking Horse locality, where stage III samples have the highest $\delta^{18}O$ and $\delta^{13}C$ values, while stage IV coarse and reddish dolomite have the lowest values. Similar trends are often ascribed to the mixing of fluids (e.g., Banner 1995; Spangenberg et al. 1996). Such a process is often supported by a salinity–temperature trend in fluid inclusion data. In our data, a salinity–temperature trend can be deduced for the sphalerite and quartz mineralization, in that higher salinity fluids generally have a corresponding lower temperature (Fig. 12). This trend can also be detected in some dolomite types; however, these data are more scattered, with a larger range in temperature. The total variation of $\delta^{13}C$ values could be explained by the temperature dependence of isotopic fractionation (of −0.034‰ per +1°C) consistent with the total range in homogenization temperatures. However, the $\delta^{13}C$ variation, especially the $\delta^{13}C$ values of stage III versus stage IV carbonate at the Kicking Horse locality, cannot be related to the variation in mean homogenization temperature of the respective carbonate types. In addition, the $\delta^{18}O$ values cannot result from temperature variation alone, and thus it is likely that the $\delta^{18}O$ range is reflecting a variation in the oxygen isotopic composition of the carbonate-precipitating fluid. Although the $\delta^{18}O$–$\delta^{13}C$ pattern in the MVT-related dolomite reported by Nesbitt and Muehlenbachs (1994) is slightly more scattered, the results of that study are similar to those in our study. In contrast, the $\delta^{18}O$ signature found in Devonian dolomite in the Western Canada Sedimentary Basin is generally higher (e.g., Al-Aasm et al. 2002; Amthor et al. 1993; Dix 1993; Machel et al. 1996; Mattes and Mountjoy 1980; Mountjoy and Amthor 1994; Mountjoy and Halim-Dihardja 1991; Mountjoy et al. 1999; Qing and Mountjoy 1994; Wendte et al. 1998; Fig. 16).

The $^{87}Sr/^{86}Sr$ ratios are covariant with the Fe content and have incrementally lower values in the Kicking Horse samples in the following order: stage III gray dolomite> stage III white dolomite and calcite>stage IV gray dolomite> stage IV white dolomite>stage IV coarse and reddish dolomite. Although the stage III gray dolomite sample at the Monarch locality is also characterized by the highest $^{87}Sr/^{86}Sr$ ratio and Fe content, the other samples do not show the correlation observed at the Kicking Horse locality. The stage III gray dolomite and a stage IV reddish dolomite sample from the Monarch locality are characterized by radiogenic Sr values (>0.714), whereas only the stage III gray dolomite and one calcite sample from the Kicking Horse locality fall above the MASIRBAS value of 0.7120 (i.e., maximum Sr isotope ratio of basinal shale in the Western Canada Sedimentary Basin as defined by Machel and Cavell 1999). This suggests that the radiogenic Sr signature could be derived from clastic sediments. Such high values were not reported by Nesbitt and Muehlenbachs (1994), who stated that the $^{87}Sr/^{86}Sr$ ratios of dolomite from the Kicking Horse and Monarch mineralization fall within the 0.709–0.712 range, which is consistent with the majority of our samples. Nevertheless, ratios of up to 0.715 indicating significant input of radiogenic ^{87}Sr, with likely sources from the underlying Cambrian and Precambrian clastics and/or the Precambrian basement, are relatively common in Devonian late-stage saddle dolomite or calcite of the Western Canada Sedimentary Basin (e.g., Buschkuehle and Machel 2002; Machel and Cavell 1999; Machel et al. 1996; Mountjoy et al. 1992, 1999; Wendte et al. 1998; Fig. 16).

Finally, the Li concentration in fluid inclusions also shows a decreasing trend from stage III minerals to stage IV gray and white dolomite and subsequently toward stage IV reddish and

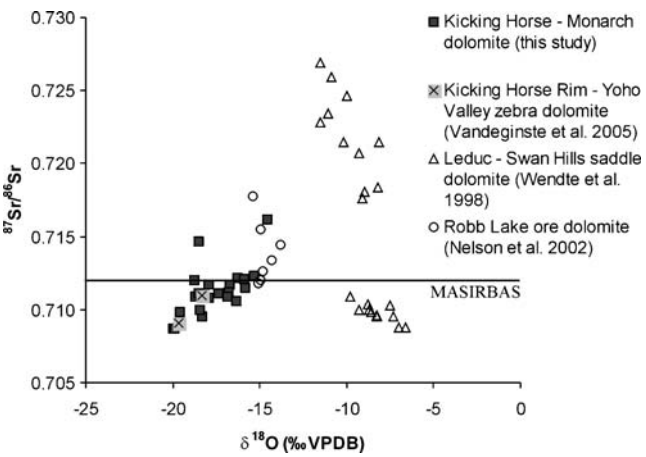

Fig. 16 $\delta^{18}O$ versus $^{87}Sr/^{86}Sr$ values from Kicking Horse and Monarch dolomite compared with published data from zebra dolomite in the neighborhood of the ore deposits, Leduc and Swan Hills saddle dolomite from the Western Canada Sedimentary Basin, and the Robb Lake ore-stage dolomite. The MASIRBAS value as defined by Machel and Cavell (1999) is indicated

coarse-crystalline white dolomite at the Kicking Horse locality. Similarly, stage III gray dolomite has a higher fluid inclusion Li concentration than stage IV dolomite at the Monarch locality. However, at this locality, the Li content is higher in reddish dolomite than in gray and white dolomite of stage IV.

In conclusion, there are chemical trends from stage III gray dolomite (with, e.g., higher Fe, Li, $^{87}Sr/^{86}Sr$) to stage IV coarse-crystalline white and reddish dolomite (with, e.g., lower Fe, Li, $^{87}Sr/^{86}Sr$), which are best exhibited at the Kicking Horse locality. We suggest these variations may be the result of a decrease in fluid–rock interaction with noncarbonate lithologies near the fluid source and along the fluid migration path and/or a progressive increase in carbonate rock buffering toward the site of deposition. Variations from this trend in terms of the $^{87}Sr/^{86}Sr$ ratio and the fluid inclusion Li content occur at the Monarch locality.

Ore formation interpretation

MVT deposits are often explained by the mixing of a saline metal-bearing fluid that leached metals from the surrounding rocks and a fluid rich in reduced sulfur, as a high concentration of metals cannot be transported easily in a fluid that also contains reduced sulfur (Beales 1975). Another model for sulfide precipitation in Pb–Zn deposits is the reduction of sulfate carried together with the metals in the ore-forming solution (Sangster 1990).

Based on the crush–leach geochemical interpretations, the Pb–Zn ore deposits of the Kicking Horse Rim could have been generated by the mixing of a fluid that obtained its salinity from the dissolution of halite (fluid A) with a seawater-evaporated basinal brine (fluid B), which has also undergone minor mixing with a dilute fluid.

End-member fluid A

The Devonian succession (possibly the Stettler/Palliser Formation or equivalents) is the most likely local source of halite. Stratigraphic equivalents occur about 2 km higher in the Paleozoic succession than the ore deposits. The ore deposits are located in large folded thrust sheets, west of the intensely imbricated zone of thrusted sheets in the Front Ranges (Faure et al. 2004). It is unlikely, therefore, that another source of evaporites could be made available by stacked thrust sheets. If the salinity source is indeed derived from the Devonian succession, then fluid A was probably cooler than fluid B, as the former originated in overlying colder strata. This is supported by the fact that the fluid inclusions in sphalerite have the lowest homogenization temperatures and the halite dissolution component was detected only in the sulfide minerals. The latter could be an indication that this fluid may have been sulfur rich.

End-member fluid B

The evaporated seawater-derived fluid (mixed with a dilute fluid) was enriched in metals scavenged from underlying clastic or basement units. The degree of interaction with siliciclastics decreases progressively within the paragenetic sequence toward the younger carbonate types (as discussed earlier). This could relate to a decreasing residence time for the evolving fluids. However, it could also be argued that there was either a decreasing contribution of the siliciclastic-derived fluids in the later stages of the paragenesis or a greater degree of buffering by carbonate host rocks. As suggested earlier, the most likely candidate responsible for the siliciclastic influence is the Lower Cambrian Gog Group arenite. Hence, fluid B may have been warmer than the surrounding rocks at the deposition site, if the fluid ascended more quickly than the rate at which it approached thermal equilibrium. This would be consistent with the suggestion by Ney (1954) and Harrison and McIlreath (1977) that the dolomite has a hydrothermal origin.

Fluid mixing

The proposed model assumes downward fluid flow (possibly driven by emergence and elevated topography), which passes through or along Devonian halite layers. In addition, a driving force that induced upward flow of basinal brines, of unknown origin, is needed. It is postulated that both fluids were channeled along fractures or faults and finally mixed at the site of deposition. Moreover, the diversity of sulfide and carbonate types and the occurrence of several periods of brecciation with broken and displaced sulfide fragments suggests that the flow of one or both fluids was probably episodic.

This interpretation of fluid flow mixing is proposed for both the Kicking Horse and Monarch deposits. The fluid inclusion microthermometric data are similar for both localities and the dolomite crush–leach data show that the mineralizing fluids at both localities have a main component of evaporated seawater origin. Nevertheless, the observed differences in the cation and isotopic data may suggest that the fluids interacted in a slightly different way with rocks along their migration path to the site of mineralization (e.g., dissolution or precipitation of certain K and Na minerals; see above).

Structural control on ore emplacement and timing?

The ore deposits at the Kicking Horse and Monarch localities are situated spatially along the Kicking Horse Rim, suggesting an influence by this facies transition on the location of ore formation. Tectonic deformation was especially well developed at this facies transition, causing deformation structures

(e.g., tectonic brecciation as well as faults or fractures) that facilitated ore emplacement. Besides the mapped Fossil Gully and Stephen–Cathedral normal faults, analysis of aerial photographs identified additional photo-lineaments in the area of the ore bodies, which may correspond to fractures or faults that developed in conjunction with the mapped faults as an extensional strain. This strain could have favored periodic intake and expulsion of fluids along fractures and faults (Sibson 2000), which acted as migration paths for downward as well as upward fluid flow and, as a result, may have facilitated the mixing zone.

The microthermometric data from this study constrain the timing of ore emplacement, to be either Ordovician–Devonian or Early Tertiary on the basis of the burial history of the area (Fig. 17) and the assumption that the fluids reached thermal equilibrium with the host rock. An Early Tertiary age is preferred because a higher degree of deformation (e.g., thick twinning planes) would be expected and fluid inclusions would be expected to exhibit more post-trapping effects if they had undergone a pre-Early Tertiary burial of up to 8 km depth. Moreover, taking into account the likely role of normal faults, an Early to Middle Eocene age could be supported (cf. Roure et al. 2005), although the age of the normal faults near the study area is not well constrained.

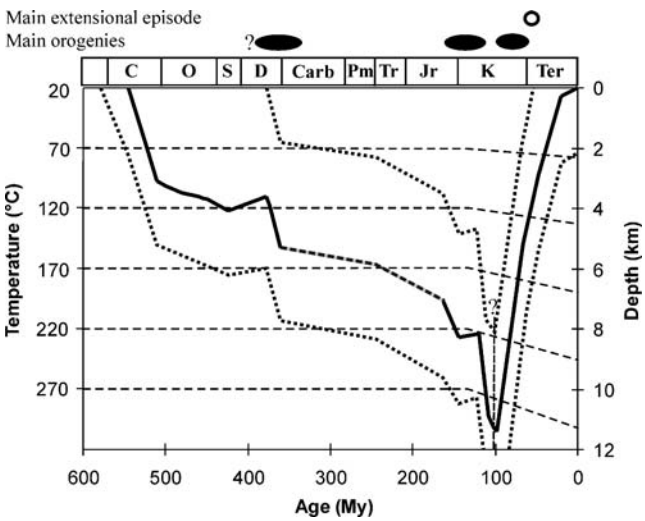

Fig. 17 Reconstructed burial temperature curve. For the temperature–depth correlation, a surface temperature of 20°C and a geothermal gradient of 25°C/km were assumed until the peak of the Columbian Orogeny and 22°C/km subsequently. Cambrian burial was based on the reconstructed curve of Bond and Kominz (1984) and checked with undecompacted stratigraphic thicknesses. For younger strata, stratigraphic thicknesses, extrapolated from well data, and erosion periods were taken into account. Tectonic loading is based on Wright et al. (1994) and Root (2001). The burial curve is consistent with Price and Fermor (1985) and Price (1994)

Comparison of Kicking Horse and Monarch with Pine Point and other MVT deposits in Western Canada

The Pine Point MVT Pb–Zn deposit is located in the Northwest Territories about 1,000 km north of the Kicking Horse and Monarch deposits and 500 km east of the Cordilleran deformation limit. This ore deposit, hosted in Devonian carbonate rocks, has been the subject of several studies on MVT ore formation, dolomitization, and fluid flow (e.g., Adams et al. 2000; Garven 1985; Gleeson and Turner 2006; Jackson and Beales 1967; Krebs and Macqueen 1984; Kyle 1981; Qing and Mountjoy 1994; Rhodes et al. 1984). Like most Devonian dolomite from the Western Canada Sedimentary Basin, the $\delta^{18}O$ values from Pine Point dolomite (−11 to −7‰ VPDB; Qing and Mountjoy 1994) are higher than those in the Kicking Horse and Monarch dolomite. The $\delta^{13}C$ values in this dolomite (−2 to +2‰ VPDB; Qing and Mountjoy 1994) are more comparable to those from the MVT deposits of our study. High $^{87}Sr/^{86}Sr$ ratios, as commonly found in Paleozoic carbonate in the Western Canada Sedimentary Basin and also in the Kicking Horse and Monarch deposits, are not detected in the Pine Point dolomite (Mountjoy et al. 1992; Qing and Mountjoy 1994). At Pine Point, fluid inclusion homogenization temperatures are generally lower in sphalerite (51–99°C) than in dolomite (85–106°C), whereas the salinities in both are similar (total range of 15–31 wt% NaCl eq.) or slightly higher in sphalerite (Gleeson and Turner 2006; Kyle 1981; Qing and Mountjoy 1994; Roedder 1968). These observations are similar to our results with the exception that in Monarch and Kicking Horse, the sphalerite-hosted inclusions tend to have lower salinities than those in dolomite. Fluid mixing was proposed for ore emplacement at Pine Point based on fluid inclusion characteristics (e.g., Adams et al. 2000; Gleeson and Turner 2006; Haynes and Kesler 1987). The predominant fluid is, similar to our samples, a brine derived from the evaporation of seawater. At Pine Point, the cation signatures in the leachates also show some evidence for interactions with clastic units or crystalline basement (Gleeson and Turner 2006), similar to our study.

The Robb Lake ore deposit is situated among a series of MVT deposits in the northern Rocky Mountains about 700 km northwest of the Kicking Horse and Monarch deposits. Coarsely crystalline sparry dolomite associated with sulfide bodies at Robb Lake ($\delta^{18}O$=−15.6 to −13.8‰ VPDB; $\delta^{13}C$=−1.6 to −0.8‰ VPDB; Nelson et al. 2002) is comparable isotopically to Monarch stage III gray dolomite. However, the other dolomite types in our study have generally lower $\delta^{18}O$ values (Fig. 16). The high $^{87}Sr/^{86}Sr$ ratios (0.7118 to 0.7178) in the Robb Lake dolomite indicate a strong influence of Rb-rich siliciclastic sedimentary rocks in the dolomitizing fluids (Nelson et al. 2002), while similar high values have also been detected in some of our samples

(mainly in stage III dolomite). There is a positive correlation between $^{87}Sr/^{86}Sr$ and $\delta^{18}O$ values for Kicking Horse carbonate, whereas this correlation is negative for, e.g., Swan Hills late-saddle dolomite (Wendte et al. 1998) and Swan Hills–Simonette carbonate (Duggan and Mountjoy 2001), which are important carbonate systems in the Western Canada Sedimentary Basin, which are, however, not associated with MVT ores (Fig. 16).

For the Oldman River MVT deposit, one of the smaller MVT deposits located closer to Kicking Horse and Monarch (about 100 km southeast of the study area), Holter (1977) argued a Laramide or post-Laramide age based on a structural analysis.

To conclude, the Kicking Horse and Monarch deposits have many characteristics in common to both the Pine Point and Robb Lake ore deposits and may have formed by similar processes. However, all the deposits have some variation in fluid characteristics and structural setting at the deposit scale.

Conclusion

The basin-platform transition exerted a major control on the location of the major Fossil Gully and Stephen–Cathedral faults and their associated minor faults. The Kicking Horse and the Monarch ore deposits formed along these faults. The faults likely provided the most favorable locus for fluid migration. It is also likely that fractures or faults developed or became reactivated at this site simultaneous with the Stephen–Cathedral and the Fossil Gully normal faults.

The ore deposits display typical MVT features characterized by a simple mineralogy of pyrite, sphalerite, and galena, accompanied by major dolomitization. Their occurrence is stratigraphically controlled in the carbonate rocks of the Middle Cambrian Cathedral Formation. The measured fluid inclusion temperatures (Th=63–182°C) and calculated salinities (21–30 wt% NaCl eq.) lie within the range of MVT fluid conditions.

Crush–leach results suggest that the main fluid component is a brine derived from the evaporation of seawater that has undergone some dilution (~20%) by a low salinity fluid. In addition, in galena- and sphalerite-hosted fluid inclusions, a halite-dissolution fluid component was detected; however, only data from two samples was collected. It is likely that one or more of the fluid components interacted with underlying siliciclastic units, based on the fluid inclusion Li data and the carbonate radiogenic Sr isotopic compositions, both of which are highest in stage III gray dolomite. Fluid–rock interaction is also indicated by K and Na values, which are higher in the Monarch samples compared to the Kicking Horse samples. This might indicate a higher influence of dissolution of K and Na feldspars at the source or along the flow path to the Monarch locality.

We propose that the ores formed as the result of the mixing of a sulfur-bearing halite-dissolution fluid with a metal-rich seawater-evaporated fluid that was, itself, mixed with ~20% of a dilute fluid. The sulfur-bearing fluid probably infiltrated downward from overlying strata, while the metal-bearing fluid ascended, probably from the underlying Gog Group. This interpretation is based on the stratigraphic setting and on the observation that the lowest homogenization temperatures and the halite-dissolution fluid component were found in sulfide. The fluids were probably released episodically (e.g., pulses), as suggested by the diverse sulfide and dolomite types and variety and styles of brecciation seen in the ores.

Acknowledgments The authors would like to thank H. Nijs for the preparation of thin sections and doubly polished wafers for fluid inclusion analysis and D. Coetermans for assistance with chemical analyses. Dr. M. Joachimski (Erlangen, Germany) is thanked for performing the stable isotope analyses and A. Kelly and V. Gallagher (East Kilbride, Scotland) for the Sr isotope measurements. Comments by Ph. Muchez on a draft version of this paper are highly appreciated. This work is sponsored by the Research Fund of the Katholieke Universiteit Leuven (OT/01/27). Parks Canada are acknowledged for permission to sample in National Parks. The crush–leach study was funded by an NSERC Discovery Grant to S. Gleeson. The authors appreciate the constructive comments of Dr. D. Leach and Dr. K. Shelton and thank also Dr. B. Lehmann for the editorial review. They helped to improve the presentation of this work.

References

Adams JJ, Rostron BJ, Mendoza CA (2000) Evidence for two-fluid mixing at Pine Point, NWT. J Geochem Explor 69–70:103–108

Aitken JD (1971) Control of lower Paleozoic sedimentary facies by the kicking horse rim, southern rocky mountains, Canada. Bull Can Pet Geol 19:557–569

Aitken JD (1978) Revised models for depositional grand cycles, Cambrian of Western Canada. Bull Can Pet Geol 26:515–542

Aitken JD (1997) Stratigraphy of the middle cambrian platformal succession, Southern Rocky Mountains. Bull Geol Surv Can 398:1–322

Al-Aasm IS, Lonnee J, Clarke J (2002) Multiple fluid flow events and the formation of saddle dolomite: case studies from the middle Devonian of the Western Canada sedimentary basin. Mar Pet Geol 19:209–217

Al-Hashimi W, Hemingway JE (1974) Recent dolomitization and the origin of the rusty crusts of Northumberland: a reply. J Sediment Petrol 44:271–274

Allan JA (1914) Geology of the field map area, British Columbia and Alberta. Geol Surv Can Memoirs 55:215–221

Amthor JE, Mountjoy EW, Machel HG (1993) Subsurface dolomites in the upper Devonian Leduc formation buildups, central part of the Rimbey–Meadowbrook trend, Alberta. Bull Can Pet Geol 41:164–185

Aulstead KL, Spencer RJ, Krouse HR (1988) Fluid inclusion and isotopic evidence on dolomitization, Devonian of Western Canada. Geochim Cosmochim Acta 52:1027–1035

Banks DA, Boyce AJ, Samson IM (2002) Constraints on the origin of fluids forming Zn–Pb–Ba deposits: evidence from the composition of fluid inclusions. Econ Geol 97:471–480

Banner JL (1995) Application of the trace element and isotope geochemistry of strontium to studies of carbonate diagenesis. Sedimentology 42:805–824

Basuki NI, Spooner ETC (2004) A review of fluid inclusion temperatures and salinities in Mississippi Valley-type Zn–Pb deposits: identifying thresholds for metal transport. Explor Min Geol 11:1–17

Beales FW (1975) Precipitation mechanisms for Mississippi Valley-type ore deposits. Econ Geol 72:487–490

Bodnar RJ (1993) Revised equation and table for determining the freezing point depression of H_2O–NaCl solutions. Geochim Cosmochim Acta 57:683–684

Boiron MC, Cathelineau M, Banks DA, Yardley BWD, Noronha F, Miller MF (1996) P–T–X conditions of late Hercynian fluid penetration and the origin of granite-hosted gold quartz veins in northwestern Iberia: a multidisciplinary study of fluid inclusions and their chemistry. Geochim Cosmochim Acta 60:43–57

Bond G, Kominz MA (1984) Construction of tectonic subsidence curves for the early Paleozoic miogeocline, southern Canadian rocky mountains: implications for subsidence mechanisms, age of breakup, and crustal thinning. Geol Soc Amer Bull 95:155–173

Bottrell SH, Yardley BWD (1988) The composition of a primary granite-derived ore fluid from S.W. England, determined by fluid inclusion analysis. Geochim Cosmochim Acta 52:585–588

Brown WL (1948) Monarch and Kicking Horse Mines. In: Can Inst Min Met Symposium on structure geology of Canadian Ore deposit, pp 231–237

Buschkuehle BE, Machel HG (2002) Diagenesis and paleofluid flow in the Devonian Southesk–Cairn carbonate complex in Alberta, Canada. Mar Pet Geol 19:219–227

Carpenter AB (1978) Origin and chemical evolution of brines in sedimentary basins. Okla Geol Surv Circ 79:60–77

Chi G, Savard MM (1997) Sources of basinal and Mississippi valley-type mineralizing brines: mixing of evaporated seawater and halite-dissolution brine. Chem Geol 143:121–125

Connolly CA, Walter LM, Baadsgaard H, Longstaffe FJ (1990) Origin and evolution of formation waters, Alberta Basin, Western Canada Sedimentary Basin. I. Chemistry. Appl Geochem 5:375–395

Cook DG (1975) Structural style influenced by lithofacies, Rocky Mountain main ranges, Alberta—British Columbia. Geol Surv Can Bull 233:73

Craig JR, Vaughan DJ (1990) Compositional and textural variations of the major iron and base-metal sulphide minerals. In: Gray PMJ, Bowyer GJ, Castle JF, Vaughan DJ, Warner NA (eds) Sulphide deposits—their origin and processing. The Institution of Mining and Metallurgy, London, UK, pp 1–16

Dix GR (1993) Patterns of burial- and tectonically controlled dolomitization in an Upper Devonian fringing-reef complex: Leduc formation, peace river arch area, Alberta, Canada. J Sediment Petrol 63:628–640

Duggan JP, Mountjoy EW (2001) Fault-controlled dolomitization at Swan Hills Simonette oil field (Devonian), deep basin west-central Alberta, Canada. Sedimentology 48:301–348

Evans TL, Campbell FA, Krouse HR (1968) A reconnaissance study of some Western Canadian lead–zinc deposits. Econ Geol 63:349–359

Faure JL, Osadetz K, Benaouali ZN, Schneider F, Roure F (2004) Kinematic and petroleum modeling of the Alberta foothills and adjacent foreland—west of Calgary. Rev Inst Fr Pét 59:81–108

Garven G (1985) The role of regional fluid flow in the genesis of the Pine Point deposits, Western Canada sedimentary basin. Econ Geol 80:307–324

Gleeson SA (2003) Bulk analyses of electrolytes in fluid inclusions. In: Samson I, Anderson A, Marshall D (eds) Fluid inclusions: analysis and interpretation. Mineralogical Association of Canada, Short Course vol. 32,Canada, pp 233–247

Gleeson SA, Turner WA (2006) Fluid inclusion constraints on the origin of the brines responsible for Pb–Zn mineralization at Pine Point and coarse non-saddle and saddle dolomite formation in southern Northwest Territories. Geofluids 7:51–68

Goldstein RH (2001) Fluid inclusions in sedimentary and diagenetic systems. Lithos 55:159–193

Goranson EA (1937) Geology of the monarch and kicking horse ore deposits, British Columbia. Econ Geol 32:471–493

Hanor JS (1996) Controls on the solubilization of lead and zinc in basinal brines. In: Sangster DF (ed) Carbonate-hosted lead–zinc deposits. Society of Economic Geologists, Special Publication, vol. 4, pp 483–500

Harrison RS, McIlreath IA (1977) Kicking Horse Pass field trip guidebook. No. 29, Canadian Society of Petroleum Geologists, Canada

Haynes FM, Kesler SE (1987) Chemical evolution of brines during Mississippi Valley-type mineralization: evidence from East Tennessee and Pine Point. Econ Geol 82:53–71

Heijlen W, Muchez P, Banks DA (2001) Origin and evolution of high-salinity, Zn–Pb mineralising fluids in the Variscides of Belgium. Miner Depos 36:165–176

Holter ME (1977) The oldman river lead–zinc occurrence, southwestern alberta. Bull Can Pet Geol 25:92–109

Jackson SA, Beales FW (1967) An aspect of sedimentary basin evolution: the concentration of Mississippi Valley-type ores during late stages of diagenesis. Bull Can Pet Geol 15:383–433

Kesler SE, Martini AM, Appold MS, Walter LM, Huston TJ, Furman FC (1996) Na–Cl–Br systematics of fluid inclusions from Mississippi Valley-type deposits, Appalachian Basin: constraints on solute origin and migration paths. Geochim Cosmochim Acta 60:225–233

Kharaka YK, Meast AS, Carothers WW, Law LM, Lamothe PJ, Fries TL (1987) Geochemistry of metal-rich brines from central Mississippi Salt Dome basin, U.S.A. Appl Geochem 2:543–561

Krebs W, Macqueen R (1984) Sequence of diagenetic and mineralization events, Pine Point lead–zinc property, Northwest Territories, Canada. Bull Can Pet Geol 32:434–464

Kyle JR (1981) Geology of Pine Point lead–zinc district. In: Wolf KH (ed) Handbook of strata-bound and stratiform ore deposits, vol. 9. Elsevier, New York, pp 643–741

Leach DL, Bradley D, Lewchuk MT, Symons DTA, de Marsily G, Brannon J (2001) Mississippi Valley-type lead–zinc deposits through geological time: implications from recent age-dating research. Miner Depos 36:711–740

Leach DL, Sangster DF, Kelley KD, Large RR, Garven G, Allen CR, Gutzmer J, Walters S (2005) Sediment-hosted Pb–Zn deposits: a global perspective. In: Hendquist J, Thompson J, Goldfarb R, Richards J (eds) Society of Economic Geology 100th Anniversary Volume, pp 561–608

Lumsden DN (1979) Discrepancy between thin section and X-ray estimates of dolomite in limestone. J Sediment Petrol 49:429–436

Machel HG, Cavell PA (1999) Low-flux, tectonically-induced squeegee fluid flow ('hot flash') into the Rocky Mountain Foreland Basin. Bull Can Pet Geol 47:510–533

Machel HG, Cavell PA, Patey KS (1996) Isotopic evidence for carbonate cementation and recrystallization, and for tectonic expulsion of fluids into the Western Canada Sedimentary Basin. Geol Soc Amer Bull 108:1108–1119

Mattes BW, Mountjoy EW (1980) Burial dolomitization of the upper devonian miette buildup, Jasper National Park, Alberta. In: Zenger DH, Dunham JB, Ethington RL (eds) Concepts and models of dolomitization. Spec Publ Soc Econ Paleontol Mineral 28:259–297

Mountjoy EW, Amthor JE (1994) Has burial dolomitization come of age? Some answers from the Western Canada sedimentary basin. In: Purser B, Tucker M, Zenger D (eds) Dolomites, a volume in honour of Dolomieu. International Association of Sedimentologists, Special Publication, vol. 21, pp 203–229

Mountjoy EW, Halim-Dihardja MK (1991) Multiple phase fracture and fault-controlled burial dolomitization, Upper Devonian Wabamun Group, Alberta. J Sediment Petrol 61:590–612

Mountjoy EW, Qing H, McNutt RH (1992) Strontium isotopic composition of Devonian dolomites, Western Canada sedimentary basin: significance of sources of dolomitizing fluids. Appl Geochem 7:59–75

Mountjoy EW, Machel HG, Green D, Duggan J, Williams-Jones AE (1999) Devonian matrix dolomite and deep burial carbonate cements: a comparison between the Rimbey–Meadowbrook reef trend and the deep basin of west-central Alberta. Bull Can Pet Geol 47:487–509

Nelson J, Paradis S, Christensen J, Gabites J (2002) Canadian Cordilleran Mississippi Valley-type deposits: a case for Devonian–Mississippian back-arc hydrothermal origin. Econ Geol 97:1013–1036

Nesbitt BE, Muehlenbachs K (1994) Paleohydrology of the Canadian Rockies and origins of brines, Pb–Zn deposits and dolomitization in the Western Canada Sedimentary Basin. Geology 22:243–246

Nesbitt BE, Prochaska W (1998) Solute chemistry of inclusion fluids from sparry dolomites and magnesites in Middle Cambrian carbonate rocks of the southern Canadian Rocky Mountains. Can J Earth Sci 35:546–555

Ney CS (1954) Monarch and Kicking Horse Mines, field, British Columbia. In: Scott JC, Fox FC (eds) Guidebook of banff–golden–radium. Alberta Society Petroleum Geologists, 4th annual field conference guidebook, pp 119–136

Plumlee GS, Leach DL, Hofstra AH, Landis GP, Rowan EL, Viets JG (1994) Chemical reaction path modeling of ore deposition in Mississippi Valley-type Pb–Zn deposits of the Ozark Region, U.S. Midcontinent. Econ Geol 89:1361–1383

Price RA (1994) Cordilleran tectonics and the evolution of the Western Canada Sedimentary Basin. In: Mossop GD, Shetsen I (eds) Geological atlas of the Western Canada Sedimentary Basin. Canadian Society of Petroleum Geologists and Alberta Research Council, Calgary, Alberta

Price RA, Fermor PR (1985) Structure section of the Cordilleran foreland thrust and fold belt west of Calgary. Geol Surv Can, Paper 84-14

Price RA, Cook DG, Aitken JD, Mountjoy EW (1980) Geology, Lake Louise (West Half), Alberta—British Columbia. Geol Surv Can, 'A' Series Map 1483A

Qing H, Mountjoy EW (1994) Formation of coarsely crystalline, hydrothermal dolomite reservoirs in the Presqu'ile Barrier, Western Canada sedimentary basin. AAPG Bull 78:55–77

Ramdohr P (1969) The ore minerals and their overgrowths. Pergamon, Oxford, UK

Rhodes D, Lantos EA, Lantos JA, Webb RJ, Owens DC (1984) Pine Point orebodies and their relationship to the stratigraphy, structure, dolomitization and karstification of the Middle Devonian Barrier Complex. Econ Geol 79:991–1055

Rittenhouse G (1967) Bromine in oil-field waters and its use in determining possibilities of origin of these waters. Am Assoc Pet Geol Bull 51:2430–2440

Roedder A (1968) Temperature, salinity and origin of the ore-forming fluids at Pine Point, Northwest Territories, Canada, from fluid inclusion studies. Econ Geol 63:439–450

Roedder E (1984) Fluid inclusions: volume 12 of Reviews in Mineralogy. Mineralogical Society of America, Chelsea, MI

Root KG (2001) Devonian antler fold and thrust belt and foreland basin development in the southern Canadian Cordillera: implications of the Western Canada sedimentary basin. Bull Can Pet Geol 49:7–36

Rosenbaum J, Sheppard SM (1986) An isotopic study of siderites, dolomites and ankerites at high temperatures. Geochim Cosmochim Acta 50:1147–1150

Roure F, Swennen R, Schneider F, Faure JL, Ferket H, Guilhaumou N, Osadetz K, Robion P, Vandeginste V (2005) Incidence and importance of tectonics and natural fluid migration on reservoir evolution in foreland fold-and-thrust belts. Rev Inst Fr Pét 60:67–106

Sangster DF (1990) Mississippi valley-type and SEDEX lead–zinc deposits: a comparative examination. Trans Inst Min Metall B Appl Earth Sci 99:21–42

Sibson RH (2000) Fluid involvement in normal faulting. J Geodyn 29:469–499

Spangenberg J, Fontboté L, Sharp ZD, Hunziker J (1996) Carbon and oxygen isotope study of hydrothermal carbonates in the zinc–lead deposits of the San Vicente district, central Peru: a quantitative modeling on mixing processes and CO_2 degassing. Chem Geol 133:289–315

Sverjensky DA (1986) Genesis of Mississippi valley-type lead–zinc deposits. Annu Rev Earth Planet Sci 14:177–199

Symons DTA, Lewchuk MT, Sangster DF (1998) Laramide orogenic fluid flow into the Western Canada Sedimentary Basin: evidence from paleomagnetic dating of the Kicking Horse Mississippi Valley-type ore deposit. Econ Geol 93:68–83

Vandeginste V, Swennen R, Gleeson SA, Ellam RM, Osadetz K, Roure F (2005) Zebra dolomitization as a result of focused fluid flow in the Rocky Mountains fold and thrust belt, Canada. Sedimentology 52:1067–1095

Veizer J, Ala D, Azmy K, Bruckshen P, Buhl D, Bruhn F, Carden GAF, Diener A, Ebneth S, Godderis Y, Jasper T, Korte C, Pawellek F, Podlaha OG, Strauss H (1999) $^{87}Sr/^{86}Sr$, $\delta^{13}C$ and evolution of Phanerozoic seawater. Chem Geol 161:59–88

Viets JG, Hofstra AH, Emsbo P (1996) Solute compositions of fluid inclusions in sphalerite from North American and European Mississippi valley-type ore deposits: ore fluids derived from evaporated seawater. In: Sangster DF (ed) Carbonate-hosted lead–zinc deposits. Society of Economic Geologists, Special Publication, vol. 4, pp 465–482

Wachter E, Hayes JM (1985) Exchange of oxygen isotopes in carbondioxide–phosphoric acid systems. Chem Geol 52:365–374

Wendte J, Qing H, Dravies JJ, Moore SLO, Stasiuk LD, Ward G (1998) High-temperature saline (thermoflux) dolomitization of Devonian Swan Hills platform and bank carbonates, wild river area, west-central Alberta. Bull Can Pet Geol 46:210–265

Wilkinson JJ (2001) Fluid inclusions in hydrothermal ore deposits. Lithos 55:229–272

Wright GN, McMechan ME, Potter DEG (1994) Chapter 3. Structure and architecture of the Western Canada Sedimentary Basin. In: Mossop GD, Shetsen I (eds) Geological atlas of the Western Canada sedimentary basin. Canadian Society of Petroleum Geologists and Alberta Research Council, Calgary, Alberta (online version)

Yang W, Spencer RJ, Krouse HR (1995) Stable isotope and major element compositions of fluid inclusions in Devonian and Cambrian dolomite cements, Western Canada. Geochim Cosmochim Acta 59:3159–3172

Yao Q, Demicco RV (1995) Paleoflow patterns of dolomitizing fluids and paleohydrology of the southern Canadian Rocky Mountains: evidence from dolomite geometry and numerical modeling. Geology 23:791–794

Yao Q, Demicco RV (1997) Dolomitization of the Cambrian carbonate platform, Southern Canadian rocky mountains: dolomite front geometry, fluid inclusion geochemistry, isotopic signature, and hydrogeologic modelling studies. Am J Sci 297:892–938